Published in final edited form as:
*Nat Immunol*. 2019 November 01; 20(11): 1517–1529. doi:10.1038/s41590-019-0490-2.

# Ikaros prevents autoimmunity by controlling anergy and Toll-like receptor signaling in B cells

**Tanja A. Schwickert**[1,#], **Hiromi Tagoh**[1,2], **Karina Schindler**[1], **Maria Fischer**[1], **Markus Jaritz**[1], **Meinrad Busslinger**[1,#]

[1]Research Institute of Molecular Pathology (IMP), Vienna Biocenter (VBC), Campus-Vienna-Biocenter 1, A-1030 Vienna, Austria

## Abstract

The establishment of a diverse B cell antigen receptor (BCR) repertoire by V(D)J recombination also generates autoreactive B cells. Anergy is one tolerance mechanism, which renders autoreactive B cells insensitive to stimulation by self-antigen, whereas Toll-like receptor (TLR) signaling can reactivate anergic B cells. Here, we describe a critical role of the transcription factor Ikaros in controlling BCR anergy and TLR signaling. Mice with specific deletion of *Ikaros* in mature B cells developed systemic autoimmunity. Ikaros regulated many anergy-associated genes, including *Zfp318* implicated in attenuation of BCR responsiveness by promoting IgD expression in anergic B cells. TLR signaling was hyperactive in Ikaros-deficient B cells, which failed to upregulate feedback inhibitors of the MyD88–NF-κB signaling pathway. Systemic inflammation was lost upon expression of a non-self-reactive BCR or loss of MyD88 in Ikaros-deficient B cells. Thus, Ikaros acts as a guardian preventing autoimmunity by promoting BCR anergy and restraining TLR signaling.

### Keywords

Ikaros; B cell anergy; TLR signaling; autoimmunity

## Introduction

B cell immunity provides acute and long-term protection of the host against infection through secretion of high-affinity antibodies that recognize an almost unlimited number of pathogens[1]. The highly diverse B cell antigen receptor (BCR) repertoire is generated by

[#]To whom correspondence should be addressed: phone: (+43/1) 797 30 − 3150 fax: (+43/1) 797 30 − 223150.
[2]Present address: Ludwig Institute for Cancer Research, University of Oxford, Oxford OX 7DQ, UK

**Data availability**
The ATAC-seq, ChIP-seq and RNA-seq data reported in this study (Table 6) are available at the Gene Expression Omnibus (GEO) repository under the accession numbers GSE122313.

**Author contributions**
T.A.S. performed almost all experiments; H.T. did the Bio-ChIP-seq experiments; K.S. performed the phosflow staining analyses; M.F. and M.J. did the bioinformatic analysis of all RNA-seq data and ChIP-seq data, respectively; T.A.S. and M.B. planned the project, designed the experiments and wrote the manuscript.

**Competing interests**
The authors declare no competing financial interests.


Europe PMC Funders Author Manuscripts

random V(D)J recombination of immunoglobulin gene segments, which inevitably creates autoreactive BCRs recognizing self-antigens[2]. About half of the emerging immature B cells in human and mouse are autoreactive[2,3], and one third of these cells are eliminated in the bone marrow by central tolerance mechanisms[4]. Autoreactive B cells in the spleen undergo peripheral tolerance by anergy induction, which keeps self-reactive B cells in check[4,5]. Anergy induction generates a non-responsive, but reversible state of the BCR by dampening the signaling responses to chronic exposure of self-antigen[5].

While loss of B cell anergy contributes to systemic inflammation, it is insufficient to cause autoimmunity, which additionally requires deregulation of other signaling systems including the nucleic acid-sensing Toll-like receptors (TLRs)[4,6]. One key factor contributing to the pathogenesis of the autoimmune disease systemic lupus erythemathosus (SLE) is defective clearance of apoptotic cell debris, which releases RNA and DNA to activate signaling of the endosomal TLR7 and TLR9, respectively[7]. Genome-wide association studies (GWAS) identified numerous susceptibility loci for SLE[7]. *IKZF1,* encoding the transcription factor Ikaros[8], is one of these risk genes[9–14]. Moreover, patients with heterozygous *IKZF1* mutations present with hypogammaglobulinemia, and a subset of them develop autoimmune disease[15–18]. Apart from these association studies, no data exist that causally implicate *IKZF1* in the pathogenesis of autoimmune disease. Here, we demonstrate that the loss of Ikaros causes systemic autoimmunity in a mouse model with selective inactivation of *Ikzf1* in B cells. Detailed molecular analyses revealed that Ikaros suppresses autoimmunity by inducing BCR anergy and restraining TLR signaling in autoreactive B cells.

## Results

### Splenomegaly upon loss of Ikaros in mature B cells

To study the role of Ikaros in peripheral B cells, we inactivated a *lox*P-flanked *Ikzf1* (*Ikzf1* $^{fl}$) allele[19] in *Cd23*-Cre *Ikzf1* $^{fl/fl}$ or *Cd23*-Cre *Ikzf1* $^{fl/–}$ mice. *Cd23*-Cre initiates gene deletion specifically in immature B cells of the spleen leading to efficient deletion in marginal zone (MZ) and follicular (FO) B cells[20]. We observed an increased spleen size in *Cd23*-Cre *Ikzf1* $^{fl/fl}$ and *Cd23*-Cre *Ikzf1* $^{fl/–}$ mice (referred to as '*Ikzf1* $^{B–}$') compared to control *Ikzf1* $^{fl/fl}$, *Ikzf1* $^{fl/–}$, *Ikzf1* $^{fl/+}$ and *Cd23*-Cre *Ikzf1* $^{fl/+}$ mice (referred to as '*Ikzf1* $^{B+}$') at the age of 5-10 weeks (Fig. 1a and Supplementary Fig. 1a). The splenomegaly in *Ikzf1* $^{B–}$ mice peaked with a 3-fold increase in spleen weight between 6 and 8 weeks (Fig. 1b). The thymus was not affected, and lymph nodes, mainly of cervical origin, showed a mild hyperplasia (Supplementary Fig. 1a). Experiments with mixed bone marrow chimeras revealed a dominant effect of the Ikaros-deficient B cells, as the spleen was already enlarged at 4 weeks after bone marrow transplantation in chimeras generated with CD45.1$^{+}$ wild-type and CD45.2$^{+}$ *Ikzf1* $^{B–}$ bone marrow (Supplementary Fig. 1b).

Flow cytometric analysis of splenocytes revealed a relative loss of conventional B-2 cells and NK cells as well as a relative increase in T cells in *Ikzf1* $^{B–}$ mice compared to *Ikzf1* $^{B+}$ mice, while the frequencies of B-1 cells, monocytes and granulocytes were unchanged at the age of 5-10 weeks (Fig. 1c and Supplementary Fig. 1c). The Ikaros protein was specifically lost only in B cells (B-1 and B-2) of *Ikzf1* $^{B–}$ mice (Fig. 1d). The loss of Ikaros was initiated in transitional T1 and T2 B cells and was complete in most (> 80%) mature B cells in *Ikzf1*

$^{B-}$mice (Fig. 1d). MZ B cells were severely (~10-fold) reduced, and FO B cells were significantly decreased in *Ikzf1* $^{B-}$ mice compared to *Ikzf1* $^{B+}$ mice (Fig. 1c,e and Supplementary Fig. 1c). CD21$^{lo/-}$CD23$^{-}$ B cells were strongly enriched in *Ikzf1* $^{B-}$ mice compared to *Ikzf1* $^{B+}$ mice (Fig. 1c,e). In mixed bone marrow chimeras, MZ B cells of the CD45.1$^{+}$ wild-type and CD45.2$^{+}$ *Ikzf1* $^{B-}$ genotypes were similarly lost, while the CD21$^{lo/-}$CD23$^{-}$ B cells of the CD45.2$^{+}$ *Ikzf1* $^{B-}$ genotype were increased compared to the respective CD45.1$^{+}$ wild-type B cells (Supplementary Fig. 1b). Hence, the loss of MZ B cells was not a B cell-intrinsic defect of Ikaros deficiency in contrast to the increase of CD21$^{lo/-}$CD23$^{-}$ B cells.

FO and CD21$^{lo/-}$CD23$^{-}$ B cells in unimmunized *Ikzf1* $^{B-}$ mice were activated as shown by high expression of MHCII and CD86, and the size of CD21$^{-}$CD23$^{-}$ B cells in *Ikzf1* $^{B-}$ mice was greatly increased compared to control B cells (Fig. 1f and Supplementary Fig. 1d). The large (FSC$^{hi}$) CD21$^{-}$CD23$^{-}$ B cells had the phenotype CD19$^{+}$CD21$^{-}$CD23$^{-}$ IgD$^{lo}$MHCII$^{hi}$CD86$^{+}$CD5$^{int}$CD11b$^{lo}$CD11c$^{lo}$CD95$^{int}$TACI$^{hi}$CXCR3$^{hi}$Blimp-1$^{lo}$T-bet$^{+}$ (Fig. 1f and Supplementary Fig. 1d), which resembles the phenotype of age-associated B cells (ABCs)[21,22]. In summary, the B cell-specific loss of Ikaros led to splenomegaly, a decrease in FO and MZ B cells, strong activation of B cells and the appearance of ABC-like cells in *Ikzf1* $^{B-}$ mice at an early age.

## Ikaros loss in B cells causes inflammation in the spleen

The splenic CD4$^{+}$ and CD8$^{+}$ T cells were increased in *Ikzf1* $^{B-}$ mice compared to *Ikzf1* $^{B+}$ mice at the age of 5-8 weeks due to a higher frequency of effector/memory T cells (CD44$^{+}$CD62L$^{-}$; Fig. 2a). This increase in activated T cells was not observed in younger (2-week-old) or older (> 18-week-old) mice (Supplementary Figs. 1c and 2a). All activated T cells in *Ikzf1* $^{B-}$ *Prdm1* $^{Gfp/+}$ mice were effector T cells (Fig. 2b), as they expressed Blimp-1 (*Prdm1*), controlling the effector T cell fate[23]. The level of interferon-γ (IFN-γ) and tumor necrosis factor (TNF) was elevated in *Ikzf1* $^{B-}$ mice compared to *Ikzf1* $^{B+}$ littermates, possibly reflecting the increase in effector T cells expressing these inflammatory cytokines (Supplementary Fig. 2b). Analysis of the architecture of *Ikzf1* $^{B-}$ spleens revealed disorganized B cell follicles lacking MZ B cells (IgM$^{hi}$IgD$^{lo}$) and containing an expanded T cell zone (CD90$^{+}$) with ectopic IgM staining (Fig. 2c, right, and Supplementary Fig. 2c). T and B cells infiltrated the liver and kidney in *Ikzf1* $^{B-}$ mice in contrast to *Ikzf1* $^{B+}$ littermates, indicating that systemic inflammation also affected non-hematopoietic organs (Supplementary Fig. 2d,e).

Germinal centers (GCs) were absent in the spleen of unimmunized *Ikzf1* $^{B-}$ mice (Supplementary Fig. 2f,g). As *Aicda*-Cre *Ikzf1* $^{fl/-}$ mice (referred to as *Ikzf1* $^{GCB-}$) with specific *Ikaros* deletion in GC B cells[20] did not develop splenomegaly (data not shown), we immunized these mice with the T cell-dependent antigen nitrophenyl-keyhole limpet hemocyanin (NP-KLH). GC B cells were strongly reduced in the spleen of immunized *Ikzf1* $^{GCB-}$ mice compared to *Ikzf1* $^{B+}$ mice, and the residual GC B cells still expressed Ikaros (Supplementary Fig. 2g), indicating a strict dependence of GC B cells on Ikaros. Long-lived Ikaros-deficient plasma cells (PCs) were absent in the bone marrow of *Ikzf1* $^{B-}$ mice, while Ikaros-deficient plasmablasts (PBs) transiently appeared in the spleen (Fig. 2d and

Supplementary Fig. 2h,i), leading to similar titers of antibody isotypes in 4-8-week-old *Ikzf1* $^{B-}$ and *Ikzf1* $^{B+}$ mice (Supplementary Fig. 2j). Anti-nuclear antibodies (ANA) were detected in *Ikzf1* $^{B-}$, but not in *Ikzf1* $^{B+}$ mice (Fig. 2e). Hence, Ikaros stringently controlled the development of GC B cells and long-lived plasma cells, while the B cell-specific loss of Ikaros caused inflammation characterized by the presence of activated B cells, increased effector T cells and autoantibodies.

## T cells promote inflammation upon Ikaros loss in B cells

As the multiple indirect effects, which cause inflammation in *Ikzf1* $^{B-}$ mice, preclude identification of the B cell-specific function of Ikaros in suppressing autoimmunity, we tried to intercept the inflammatory cascade by eliminating causative cell types. We deleted antibody-secreting cells in *Ikzf1* $^{B-}$ mice by eliminating the plasma cell regulator Blimp-1 (*Prdm1*)[1] in *Cd23*-Cre *Ikzf1* $^{fl/fl}$ *Prdm1* $^{Gfp/fl}$ or *Cd23*-Cre *Ikzf1* $^{fl/fl}$ *Prdm1* $^{fl/fl}$ mice (referred to as *Ikzf1* $^{B-}$ *Prdm1* $^{B-}$). The absence of antibody-secreting cells did not prevent inflammation, as documented by the observed splenomegaly, absent MZ B cells, decreased FO B cells and increased activated T and CD21$^{lo/-}$CD23$^{-}$ B cells in *Ikzf1* $^{B-}$ *Prdm1* $^{B-}$ mice (Supplementary Fig. 3a,b).

We next eliminated αβ T cells by deleting the Eβ enhancer of the *Tcrb* locus in Eβ$^{-/-}$ *Ikzf1* $^{B-}$ mice (Supplementary Fig. 3c). These mice did not develop splenomegaly (Fig. 3a), had normal frequencies of MZ and FO B cells and contained low numbers of CD21$^{lo/-}$CD23$^{-}$ B cells at the age of 5-6 weeks (Fig. 3b and Supplementary Fig. 3c). Hence, the inflammation in *Ikzf1* $^{B-}$ mice depended on αβ T cells, which caused the loss of MZ and FO B cells in a non-B-cell-intrinsic manner.

To determine whether CD4$^{+}$ or CD8$^{+}$ T cells cause the inflammation, we generated chimeric mice by reconstituting B-cell-deficient $J_HT$ (*Igh* $^{?Jh/?Jh}$) mice[24] with *Ikzf1* $^{B-}$ or control *Ikzf1* $^{B+}$ bone marrow and subsequently deleted CD4$^{+}$ or CD8$^{+}$ T cells by intravenous injection of neutralizing anti-CD4 or anti-CD8 antibodies at regular intervals prior to flow cytometric analysis at 5 weeks post transplantation. Only the deletion of CD4$^{+}$ T cells in the *Ikzf1* $^{B-}$ bone marrow chimeras prevented splenomegaly and the generation of CD21$^{lo/-}$ CD23$^{-}$ B cells, while promoting normal development of MZ B cells (Fig. 3c,d and Supplementary Fig. 3d). Hence, CD4$^{+}$ T cells contribute to the inflammation in *Ikzf1* $^{B-}$ mice.

To investigate whether the inflammation depends on T cell receptor (TCR) specificity, we generated chimeric mice by transplanting bone marrow from T-cell-deficient Eβ$^{-/-}$ *Ikzf1* $^{B-}$ or Eβ$^{-/-}$ *Ikzf1* $^{B+}$ donor mice into three strains of sub-lethally irradiated B-cell-deficient mice, which either generated polyclonal T cells in $J_HT$ hosts, no T cells in *Rag2*$^{-/-}$ hosts or monoclonal, ovalbumin-specific CD4$^{+}$ T cells in OT-II TCR-tg *Rag2*$^{-/-}$ hosts (Fig. 3e,f). At 4-5 weeks post transplantation, the Eβ$^{-/-}$ *Ikzf1* $^{B-}$ B cells induced inflammation only in the polyclonal T cell-bearing $J_HT$ host mice (Fig. 3e,f and Supplementary Fig. 3e). In contrast, Eβ$^{-/-}$ *Ikzf1* $^{B-}$ B cells failed to induce inflammation in host mice with monoclonal CD4$^{+}$ (OT-II TCR-tg) T cells, as demonstrated by a normal spleen size, rescued MZ and FO B cell numbers, decreased CD21$^{lo/-}$CD23$^{-}$ B cells and little effector T cells (Fig. 3e,f and Supplementary Fig. 3e). Hence, the inflammation in *Ikzf1* $^{B-}$ mice was caused by the

interaction of Ikaros-deficient B cells with polyclonal $CD4^+$ T cells, which led to mutual activation of both cell types.

## A monoclonal BCR prevents inflammation in *Ikzf1* $^{B-}$ mice

We hypothesized that the inflammatory B-T cell interaction in *Ikzf1* $^{B-}$ mice depends on the recognition of self-antigen by the antigen receptors on both B and T cells. Antigen-presentation assays supported this idea, as OT-II peptide-loaded FO B cells and $CD21^{lo/-}$ $CD23^-$ B cells from the inflamed spleen of *Ikzf1* $^{B-}$ mice could induce activation and proliferation of naïve $CD4^+$ OT-II TCR-tg T cells in contrast to OT-II peptide-loaded FO B cells from control *Ikzf1* $^{B+}$ mice (Supplementary Fig. 4a). To provide direct evidence for the B-T cell interaction hypothesis, we analyzed *Ikzf1* $^{B-}$ mice expressing the MD4 BCR transgene (MD4 BCR-tg), which codes for a hen egg lysozyme (HEL)-specific BCR[25]. The MD4 BCR-tg *Ikzf1* $^{B-}$ mice had a normal spleen size, normal frequencies of MZ and FO B cells, low numbers of effector T cells and $CD21^{lo/-}CD23^-$ B cells and a normal splenic architecture (Fig. 4a,b and Supplementary Fig. 4b). Expression of the MD4 BCR-tg did not influence the kinetics of Ikaros loss from T1 to mature $CD93^-$ B cells (Fig. 4c). Hence, the replacement of a polyclonal BCR repertoire with a monoclonal, non-self-reactive BCR was sufficient to suppress inflammation triggered by Ikaros deficiency in B cells.

As the absence of inflammation in MD4 BCR-tg *Ikzf1* $^{B-}$ mice allowed us to study the direct effects of Ikaros loss, we compared the expression of several cell surface proteins on B cells of MD4 BCR-tg *Ikzf1* $^{B-}$ and MD4 BCR-tg *Ikzf1* $^{B+}$ mice (Supplementary Fig. 4c). Expression of the IgM and IgD isoforms of the BCR was deregulated in the absence of Ikaros (Fig. 4d,e). Ikaros-deficient MZ B cells expressed both BCR isoforms at a lower level than Ikaros-expressing MZ B cells. In contrast, IgM expression was increased, and IgD expression was decreased on Ikaros-deficient relative to control FO B cells (Fig. 4e). These data therefore indicated a critical role of Ikaros in regulating IgM and IgD expression in mature B cells.

## Ikaros induces anergy upon chronic antigen exposure

We next investigated whether Ikaros directly controls signaling downstream of the BCR in FO B cells of MD4 BCR-tg *Ikzf1* $^{B-}$ mice. *In vitro* stimulation of naïve FO B cells with anti-IgM or HEL antigen revealed that intracellular signal transducers (SYK, BLNK, PLCγ2, ERK1/2, AKT and S6) downstream of the BCR were equally phosphorylated in Ikaros-deficient and Ikaros-expressing B cells (Supplementary Fig. 5a). Intracellular calcium mobilization upon anti-IgM or HEL stimulation was also similar in naïve B cells lacking or expressing Ikaros (Fig. 5a and Supplementary Fig. 5b). Hence, Ikaros did not control acute BCR signaling in naïve B cells despite different IgM and IgD expression on Ikaros-deficient and control FO B cells.

The random V(D)J rearrangements in early B cell development lead to the generation of self-reactive BCRs and subsequent emergence of autoreactive B cells in the spleen[2]. These autoreactive B cells are silenced by anergy, which leads to unresponsiveness of the BCR upon chronic exposure to self-antigen[5]. To investigate whether Ikaros-deficient B cells fail to undergo anergy induction upon prolonged antigen exposure, we activated the HEL-specific

MD4 receptor by intravenous injection of monovalent HEL into MD4 BCR-tg *Ikzf1* $^{B-}$ and MD4 BCR-tg *Ikzf1* $^{B+}$ mice. Ikaros-expressing FO B cells downregulated IgM expression already at day 1 after HEL injection, while maintaining IgD expression even after 3 days (Fig. 5b), which is the typical response of MD4 BCR-tg B cells to anergy induction[25,26]. In contrast, IgM expression was only moderately downregulated on Ikaros-deficient FO B cells, while IgD expression was upregulated, although it did not reach the same IgD level detected on control FO B cells at day 3 after HEL injection (Fig. 5b). The observed deregulation of IgM and IgD expression on Ikaros-deficient FO B cells suggested that anergy induction is defective in the absence of Ikaros.

We next measured intracellular calcium mobilization in FO B cells from MD4 BCR-tg *Ikzf1* $^{B-}$ and MD4 BCR-tg *Ikzf1* $^{B+}$ mice one day after HEL injection. While intracellular calcium fluxes were strongly attenuated in Ikaros-expressing B cells upon acute stimulation with both anti-IgM or HEL, calcium signaling remained as effective in antigen-exposed Ikaros-deficient B cells as in naïve B cells, indicating that Ikaros was required for anergy induction (Fig. 5c and Supplementary Fig. 5b,c). The discrepancy in calcium signaling was, however, not caused by a difference in HEL occupancy on MD4 BCR-tg *Ikzf1* $^{B-}$ and MD4 BCR-tg *Ikzf1* $^{B+}$ B cells (Supplementary Fig. 5d).

Anergy is fully induced in B cells of MD4,ML5 double-transgenic mice, which co-express the HEL-specific MD4 BCR with its cognate antigen HEL (from the ML5 transgene)[25,26]. IgM expression was normally downregulated in splenic T1 cells of MD4,ML5 double-transgenic *Ikzf1* $^{B-}$ mice (Fig. 5d), indicating that anergy was correctly induced in these immature B cells, which had not yet undergone Cre-mediated deletion of *Ikzf1* (Supplementary Fig. 5c). In contrast, the Ikaros-deficient FO B cells of MD4,ML5 double-transgenic *Ikzf1* $^{B-}$ mice failed to fully downregulate IgM expression relative to the FO B cells of double-transgenic *Ikzf1* $^{B+}$ littermates (Fig. 5d and Supplementary Fig. 5c). Notably, intracellular calcium mobilization upon anti-IgM or HEL treatment was stronger in FO B cells from MD4,ML5 double-transgenic *Ikzf1* $^{B-}$ mice compared to double-transgenic *Ikzf1* $^{B+}$ littermates (Fig. 5e and Supplementary Fig. 5b). These data indicate that, while Ikaros was not essential for BCR signaling in naïve B cells, it was required for the initiation and maintenance of anergy in autoreactive B cells.

## Ikaros-dependent gene regulation in anergic B cells

RNA-sequencing was performed with Ikaros-deficient (MD4 BCR-tg *Ikzf1* $^{B-}$) and control (MD4 BCR-tg *Ikzf1* $^{B+}$) FO B cells that were isolated before (naïve) or after 1 day of HEL injection (Supplementary Fig. 6a,b). Comparison of the RNA-seq data between naïve Ikaros-deficient and control FO B cells identified 52 Ikaros-activated and 61 Ikaros-repressed genes with an expression difference of > 2-fold (Supplementary Fig. 6c and Table 1). A similar analysis revealed 76 Ikaros-activated and 193 Ikaros-repressed genes in HEL-exposed FO B cells (Supplementary Fig. 6d and Table 2). As a significant correlation with a Pearson coefficient of 0.67 was observed for the Ikaros-dependent gene expression changes between naïve and HEL-exposed FO B cells (Supplementary Fig. 6e), we combined all Ikaros-regulated genes, which defined an Ikaros-dependent gene signature consisting of 90 Ikaros-activated and 198 Ikaros-repressed genes in FO B cells (Fig. 6a and Table 3). The average

$log_2$-fold change of all Ikaros-regulated genes was two-fold higher in HEL-exposed FO B cells compared to naïve FO B cells (Supplementary Fig. 6e), as exemplified by the activated *Apoe* and repressed *Ctnnd1* genes (Fig. 6b). Annotation of all regulated genes revealed a 3-fold enrichment of metabolic genes in Ikaros-repressed genes and a 3-fold enrichment of genes encoding transcriptional regulators in Ikaros-activated compared to Ikaros-repressed genes (Supplementary Fig. 6f and Table 3). Genome-wide binding of Ikaros was determined in naïve FO B cells by Bio-ChIP-sequencing[19] (Fig. 6b). These analyses revealed that 53% of the activated genes and 57% of the repressed genes were bound by Ikaros and thus qualified as potentially directly regulated Ikaros target genes (Table 3), as shown for *Ctnnd1* (Fig. 6b).

By comparing RNA-seq data of fully anergic MD4,ML5 double-transgenic FO B cells and naïve MD4 BCR-tg FO B cells, we defined an anergy expression signature consisting of 59 genes with increased expression (‘anergy up’) and 50 genes with decreased expression (‘anergy down’) in anergic FO B cells relative to naïve B cells (Fig. 6a and Supplementary Fig. 6g (lower part); Table 4). This anergy expression signature correlated well with a published expression signature[27] (Supplementary Fig. 6g, upper part). Comparison of the Ikaros-dependent gene expression pattern with this anergy expression signature revealed that Ikaros-activated genes were enriched among the ‘anergy-up’ genes and Ikaros-repressed genes among the ‘anergy-down’ genes (Fig. 6a and Supplementary Fig. 6h).

Ikaros regulated a large proportion (42%) of the 109 identified anergy signature genes, containing 19 Ikaros-activated and 26 Ikaros-repressed genes (Fig. 6c). Representative repressed Ikaros target genes with strong downregulation in anergic B cells code for the cell surface proteins Endoglin (Eng), Tmem176b, Slamf9 and Sirpα and the metabolic enzyme Alox5ap (Fig. 6c,d). Activated Ikaros target genes with strong upregulation in anergic B cells code for the BCR-inducible transcription factors Nr4a1(Nur77), Bhlhe40, Egr3 and Egr coregulator Nab2 as well as for the zinc finger protein Zfp318 (Fig. 6c,d), which controls IgD expression by promoting the generation of *Ighd* mRNA[28,29]. Notably, the reduced *Zfp318* expression in Ikaros-deficient FO B cells correlated with a similar decrease in *Ighd* mRNA (Supplementary Fig. 6i). These molecular analyses identified a critical role of Ikaros in controlling B cell anergy by regulating a large part of the anergy expression program.

## Ikaros prevents TLR-mediated hyperactivation of B cells

As innate Toll-like receptors (TLRs) are known to cooperate with adaptive immune receptors in the development of autoimmunity[4,30], we investigated whether Ikaros controls TLR signaling. Ikaros-deficient (MD4 BCR-tg *Ikzf1* $^{B-}$) and control (MD4 BCR-tg *Ikzf1* $^{B+}$) FO B cells, which expressed high levels of *Tlr9* mRNA followed by lower expression of *Tlr1*, *Tlr2*, *Tlr7* and *Tlr4* (Supplementary Fig. 7a), were stimulated with Pam3 (TLR1/2 ligand), LPS (TLR4 ligand), Resiquimod R848 (TLR7 ligand) and CpG oligodeoxynucleotides (TLR9 ligand) for 4 days. Treatment with these ligands resulted in increased cell proliferation (CellTrace Violet dilution), more efficient blasting (cell size increase) and enhanced activation (CD69 expression) of Ikaros-deficient FO B cells compared to control FO B cells, in contrast to co-stimulation with anti-IgM and IL-4 or anti-CD40 (Fig. 7a). A time course analysis of LPS, R848 or CpG stimulation revealed that

hyperactivation of Ikaros-deficient B cells was detectable already at day 2 (Supplementary Fig. 7b). Hence, Ikaros restrained B cell activation in response to TLR signaling, suggesting that the TLR-induced hyperactivation of Ikaros-deficient FO B cells may contribute to the autoimmune phenotype of *Ikzf1* $^{B-}$ mice.

TLR9 signaling restricts the survival of autoreactive B cells[31] in the context of ongoing BCR signaling[32]. We therefore stimulated Ikaros-deficient and control FO B cells for up to 4 days with a stimulatory CpG-HEL immune complex (SCHIC; Supplementary Fig. 7c) that can activate the endosomal TLR9 only upon BCR signaling and internalization as described for the STIC9 complex[32]. After 4 days of SCHIC stimulation, most (70-80%) control FO B cells were dead (Supplementary Fig. 7d,e), consistent with published data[32]. In contrast, 80% of the Ikaros-deficient FO B cells were not only alive and proliferated, but also blasted more efficiently than the remaining live control B cells (Supplementary Fig. 7d,e). Hence, the loss of Ikaros prevented the post-proliferative death of FO B cells upon BCR and TLR9 activation by immune complexes.

RNA-seq comparison of Ikaros-deficient and control FO B cells after 1 day of CpG stimulation identified 129 Ikaros-activated and 136 Ikaros repressed genes (Fig. 7b and Table 5). Most Ikaros-repressed (69%) and Ikaros-activated genes (89%) were regulated only in CpG-stimulated B cells (Supplementary Fig. 8a). Annotation of the identified genes revealed a 3.2-fold enrichment of metabolic genes in Ikaros-repressed compared to Ikaros-activated genes (Supplementary Fig. 8c and Table 5), suggesting that their derepression may increase the metabolic fitness and thus blasting of Ikaros-deficient FO B cells (Fig. 7a and Supplementary Fig. 8b). CpG stimulation for 1 day significantly activated the *Irak3*, *Tnfaip3* and *Traf1* genes in control FO B cells, but not in Ikaros-deficient FO B cells (Fig. 7c), which was confirmed for TNFAIP3 protein expression in response to CpG (TLR9) and R848 (TLR7) stimulation (Supplementary Fig. 8c). Ikaros binding was detected at all three genes (Fig. 7d and Supplementary Fig. 8d), which code for feedback inhibitors restricting NF-κB activation downstream of TLRs[33–36]. While the ATAC-seq pattern at these activated genes was similar in CpG-stimulated Ikaros-deficient and control FO B cells, it differed for repressed Ikaros target genes, as exemplified by *Fes*, *Wnt10b*, *Aif1*, *Tmem176b*, *Wnt10a*, *Rassf4* and *Serpinf1* (Fig. 7d and Supplementary Fig. 8d). New open chromatin regions appeared in CpG-stimulated Ikaros-deficient B cells predominantly, but not exclusively, at sites where Ikaros was bound in control B cells, suggesting that Ikaros prevents the formation of open chromatin at its repressed target genes. In summary, the Ikaros-activated expression of three feedback inhibitors of NF-κB signaling could explain the hyperactivation of TLR signaling in Ikaros-deficient FO B cells.

We next studied the kinetics of NF-κB activation by flow cytometric measurement of the inhibitory protein IκBα in Ikaros-deficient and control FO B cells at different time points after CpG stimulation. Ikaros-deficient B cells degraded IκBα more rapidly at 15 minutes and, after full degradation at 30 minutes, expressed higher levels of IκBα at day 1 compared to control B cells (Fig. 7e). Hence, the loss of Ikaros altered the oscillatory control of NF-κB activity upon CpG stimulation. To investigate whether hyperactivation of NF-κB signaling downstream of the TLR-proximal adaptor protein MyD88 is causally involved in the development of inflammation in *Ikzf1* $^{B-}$ mice, we additionally deleted a conditional *Myd88*

$^{fl}$ allele[37] in mature B cells. Loss of MyD88 in heterozygous *Myd88* $^{B+/-}$ *Ikzf1* $^{B-}$ mice (*Cd23*-Cre *Myd88* $^{+/fl}$ *Ikzf1* $^{fl/fl}$) and homozygous *Myd88* $^{B-/-}$ *Ikzf1* $^{B-}$ mice (*Cd23*-Cre *Myd88* $^{fl/fl}$ *Ikzf1* $^{fl/fl}$) resulted in a dose-dependent decrease of the spleen size, effector/memory T cells and CD21$^{lo}$CD23$^{-}$ B cells, while rescuing FO and MZ B cell numbers (Fig. 7f and Supplementary Fig. 8d). Hence, deregulation of NF-κB signaling downstream of MyD88 is essential for the development of autoimmunity in *Ikzf1* $^{B-}$ mice.

## Discussion

Here, we have shown that the specific loss of Ikaros in mature B cells activated self-reactive B and T cells, leading to an autoimmune phenotype that peaked at 6-8 weeks in *Ikzf1* $^{B-}$ mice. The development of autoimmunity depended on self-antigen-mediated B-T cell interactions, as it was abrogated by replacing the polyclonal TCR or BCR repertoire with monoclonal, non-self-reactive antigen receptors. By presenting autoantigens on MHCII, Ikaros-deficient B cells could directly activate 'wild-type' CD4$^{+}$ T cells to differentiate into Blimp-1-expressing effector T cells[23]. As effector T cells upon prolonged inflammation become exhausted[38], it is conceivable that T cell exhaustion could explain the loss of autoimmunity in *Ikzf1* $^{B-}$ mice with progressing age. Thymic emigrants arriving in the spleen decrease after 6 weeks of age[39], which may also contribute to the transient development of autoimmunity in *Ikzf1* $^{B-}$ mice.

The absence of long-lived plasma cells in the bone marrow of *Ikzf1* $^{B-}$ mice indicated a critical role of Ikaros in their development. Ikaros-deficient plasmablasts were transiently generated in the spleen, leading to autoreactive antibodies, which, however, did not contribute to the inflammation in *Ikzf1* $^{B-}$ mice, as additional loss of the plasma cell regulator Blimp-1[1] could not rescue the autoimmune phenotype, consistent with similar findings made in lupus-prone MRL-*Fas* $^{lpr}$ mice[40]. Systemic inflammation results in the loss of MZ B cells[41], which likely explains the non-cell-autonomous loss of these cells in *Ikzf1* $^{B-}$ mice. The non-B-cell-intrinsic decrease of Ikaros-deficient FO B cells may reflect a shortened half-life due to their constant activation in inflamed *Ikzf1* $^{B-}$ mice. The loss of Ikaros affected two splenic B cell types in a cell-autonomous manner, i.e. the appearance of CD21$^{-}$CD23$^{-}$ B cells and the absence of GC B cells in *Ikzf1* $^{B-}$ mice. The Ikaros-deficient CD21$^{-}$CD23$^{-}$ B cells expressed T-bet (*Tbx21*) and exhibited a cell surface phenotype reminiscent of that of the age-associated B cells (ABCs), which appear with autoimmunity in human and mouse[21,22]. Mice with GC B-cell-specific *Ikaros* deletion did neither develop autoimmunity nor GC B cells, indicating that Ikaros loss stringently blocked GC B cell development in *Ikzf1* $^{B-}$ mice. As GC B cells play an important role in autoimmune disease progression[42], their absence could explain why the autoimmunity in *Ikzf1* $^{B-}$ mice did not develop into an autoimmune disease.

While Ikaros directly regulates pre-BCR signaling in early B lymphopoiesis[19], it did not control proximal BCR signaling in mature B cells, indicating that Ikaros fulfills distinct functions in early and late B cell development. Ikaros induced, however, anergy in autoreactive B cells. Anergy induction was extensively studied in HEL-specific MD4-BCR-tg mice, as their B cells upon chronic HEL exposure adopt an anergic phenotype, leading to BCR unresponsiveness due to strong IgM downregulation, while IgD expression remains

high[25,26]. IgD is less sensitive to autoantigens than IgM *in vivo* [43], which may be caused by distinct structural properties of the IgD receptor[44], by clustering of IgD and IgM in different protein islands on resting B cells[45] or by differential association of the two BCR receptors with activating and inhibitory co-receptors[46]. The loss of Ikaros reversed the IgM-to-IgD ratio by increasing IgM and decreasing IgD expression on FO B cells. As signaling through IgM rather than IgD leads to efficient calcium release[43,44], the high IgM expression on MD4-tg *Ikzf1* $^{B-}$ FO B cells is likely responsible for the unabatedly high calcium signaling upon HEL exposure. Gene expression analysis revealed that Ikaros controlled a large part of the anergy-associated gene expression signature. One of the directly activated Ikaros target genes, *Zfp318*, codes for a zinc finger protein that regulates IgD expression by preventing transcription termination at the 3' end of *Ighm*, which facilitates synthesis of the complete *Ighm-Ighd* precursor RNA and subsequent generation of the mature *Ighd* mRNA by alternative splicing[28,29]. Heterozygous loss of *Zfp318* leads to an increase of IgM and decrease of IgD expression on naïve mature B cells[28], similar to what we observed for Ikaros-deficient FO B cells. Other activated Ikaros target genes encode the transcriptional regulators Bhlhe40, Ets2, Egr3, Nab2 and Nr4a1(Nur77), which are induced as immediate early genes in response to acute BCR signaling[3]. These transcription factors may contribute to the control of B cell anergy as negative feedback regulators of BCR signaling, given that the loss of Bhlhe40 and Egr3 was associated with autoimmunity[47,48] and Nr4a1 expression was correlated with BCR unresponsiveness in anergic wild-type B cells[3].

Self-reactive B cells play an important role in autoimmunity by endocytosing nucleic acid-protein complexes, released from dying cells, via their autoreactive BCRs and by presenting them to TLR7 and TLR9 in the endosome, thereby activating these receptors[30]. TLR signaling was hyperactivated already in non-self-reactive Ikaros-deficient B cells of MD4-tg *Ikzf1* $^{B-}$ mice. Three activated Ikaros target genes, *Irak3, Tnfaip3* and *Traf1*, whose expression was no longer induced in Ikaros-deficient FO B cells upon TLR9 stimulation, code for feedback inhibitors of NF-κB signaling by interfering with signaling complexes at different levels downstream of TLRs. IRAK3(IRAK-M) acts at the MyD88 complex by inhibiting IRAK1/4 phosphorylation and dissociation[33]. TNFAIP3 (A20) functions as a deubiquitinase by removing polyubiquitin chains from TRAF6, which prevents further signal transduction[34,35]. By binding to the LUBAC complex, TRAF1 interferes with linear ubiquitination and thus activation of NEMO, the regulatory subunit of the IκB kinase (IKK) complex[36]. Complete loss of each of these inhibitors results in autoimmunity[33-36,49]. As heterozygous *Tnfaip3* and *Traf1* mice show a dose-dependent phenotype[34–36], it is conceivable that the combined effect of decreased *Irak3*, *Tnfaip3* and *Traf1* expression in CpG-stimulated Ikaros-deficient B cells is responsible for the observed hyperactivity of TLR signaling in these cells. Consistent with this idea, B-cell-specific loss of the TLR-proximal adaptor protein MyD88 prevented the development of autoimmunity in *Ikzf1* $^{B-}$ mice. Hence, the continuous activity of self-reactive BCRs due to the loss of anergy and the hyperreactivity of TLR signaling due to the lack of feedback inhibition are the two primary defects caused by Ikaros loss in B cells that promote systemic autoimmunity.

The discovery of two Ikaros-dependent mechanisms suppressing autoimmunity begs the question whether Ikaros is also relevant for preventing autoimmune disease in humans. *IKZF1* was identified by GWAS as a risk gene for human SLE[9–14]. Fifteen heterozygous

*IKZF1* germline mutations were discovered in a new form of common variable immunodeficiency (CVID), characterized by hypogammaglobulinemia and progressive B cell loss, while 7 of 31 patients additionally developed an autoimmune disease[15–18]. Most *IKZF1* alterations are missense mutations in one of the N-terminal zinc fingers, which abrogate DNA-binding of Ikaros[15–18]. As these mutant Ikaros proteins contain an intact C-terminal dimerization domain, they may function as dominant-negative proteins by sequestering the wild-type protein into a DNA-binding-incompetent complex. However, the mouse *Ikzf1* null mutation lacking the C-terminal dimerization domain acts as a recessive allele, which could explain the absence of an autoimmune phenotype in heterozygous *Ikzf1* $^{+/-}$ mice.

B cells play a pivotal role in the pathology of autoimmune diseases, as genetic deletion of B cells in lupus-prone MRL-*Fas* $^{lpr}$ mice prevents disease development[50]. Dual engagement of TLR and BCR signaling in autoreactive B cells has been implicated in the initiation of autoimmunity[4,30]. Our study has now provided mechanistic insight into this process by demonstrating that the B-cell-specific loss of a single transcription factor, Ikaros, which controls B cell anergy and TLR feedback inhibition, is sufficient to promote autoimmunity.

## Online Methods

### Mice

The following mice were maintained on the C57BL/6 genetic background: *Ikzf1* $^{fl/fl}$ [19], *Ikzf1* $^{+/-}$ [51], *Ikzf1* $^{ihCd2/ihCd2}$ [19], *Prdm1* $^{Gfp/+}$ [52], *Prdm1* $^{fl/fl}$ [53], Eβ$^{-/-}$ [54], $J_HT$ (*Igh* $^{?Jh/?Jh}$) [24], *Myd88* $^{fl/fl}$ [37], *Rag2* $^{-/-}$ [55], *Rosa26* $^{BirA/BirA}$ [56], OT-II TCR-tg [57], MD4 BCR-tg [25], ML5-tg [25], *Cd23*-Cre [20] and *Aicda*-Cre [20]. All animal experiments were carried out according to valid project licenses, which were approved and regularly controlled by the Austrian Veterinary Authorities.

### Antibodies

The following monoclonal antibodies were used for flow cytometry: B220/CD45R (RA3-6B2), CD3ε (145-2C11), CD4 (GK1.5), CD5 (53-7.3), CD8α (53-6.7), CD11b/Mac1 (M1/70), CD19 (1D3), CD21 (7G6), CD22 (Cy34.1), CD23 (B3B4), CD28 (37.51), CD44 (IM7), CD62L (MEL-14), CD69 (H1.2F3), CD80 (16-10A1), CD86 (GL1), CD90.2/Thy1.2 (30-H12), CD93 (AA4.1), CD95/Fas (Jo2), CD115/CSF1R (AFS98), CD138 (281-2), CXCR3 (1C6/CXCR3), HEL (HyHEL9), F4/80 (CI:A3-1), GL7 (GL7), Gr1 (RB6-8C5), IgD (11-26c.2a), IgM (II/41), $IgM^a$ (MA-69), MHCI (28-14-8, KH95, AF6-88.5), MHCII (M5-114.15.2), NK1.1 (PK136), Taci (8F10), TCRβ (H57-597), and TCRγδ (GL3).

The following antibodies were used for intracellular staining and phospho-specific flow cytometry: Ikaros (2A9; BioLegend); IκBα (rabbit polyclonal Ab; Cell Signaling Technology), phospho-AKT (p-Ser473) (D9E; Cell Signaling Technology), phospho-BLNK (p-Tyr84) (J117-1278; BD), phospho-PLCγ2 (p-Tyr759) (K86-689.37; BD), phospho-SYK (p-Tyr525/526) (C87C1; Cell Signaling Technology), phospho-ERK1/2 (p-Thr202/204) (20A; BD) and phospho-S6 (p-Ser235/236) (D57.2.2E; Cell Signaling Technology). For immunofluorescence analysis (shown in Figs. 2c,4d and Supplementary Figs. 2c,g; 4b), the

following antibodies were used: B220/CD45R-Alexa647 (RA3-6B2), CD3ε-BV421 (145-2C11), CD35-Bio (8C12), CD90- BV421 (Ox-7), IgD-Alexa488 (11-26c.2a), IgM-PE/APC (II/41), TCRβ-BV421 (H57-597), CD169-Bio (MOMA-1).

### Definition of cell types by flow cytometry

Monocytes ($CD115^+$), granulocytes ($Gr1^+$), NK cells ($TCR\beta^-NK1.1^+$), B-1 cells ($CD19^{hi}CD5^+$ or $CD19^{hi}B220^{lo}$), B-2 cells ($CD19^+CD5^-CD138^-$), mature B-2 cells ($CD19^+CD5^-CD93^-CD138^-$), T cells ($TCR\beta^+$ or $CD4^+$ plus $CD8^+$), splenic naïve $CD4^+$ T ($TCR\beta^+CD4^+CD8^-CD44^-CD62L^+$), activated $CD4^+$ T ($TCR\beta^+CD4^+CD8^-CD44^+CD62L^-$), splenic naïve $CD8^+$ T ($TCR\beta^+CD4^-CD8^+CD44^-CD62L^+$), activated $CD8^+$ T ($TCR\beta^+CD4^-CD8^+CD62L^-CD44^+$), T1 B ($CD19^+CD5^-CD93^+CD23^-$), T2 B ($CD19^+CD5^-CD93^+CD23^+$), FO B ($CD19^+CD5^-CD93^-CD23^+CD21^{lo}$), MZ B ($CD19^+CD5^-CD93^-CD21^+CD23^{lo}$), GC B cells ($CD19^+B220^+GL7^+Fas^+$), plasmablasts ($FSC^{hi}CD138^+$), plasma cells ($FSC^{hi}B220^{-/int}CD138^+$). Flow cytometry experiments and FACS sorting were performed on LSR Fortessa (BD Biosciences) and FACSAria III (BD Biosciences) machines, respectively. Flowjo software (Treestar) was used for data analysis.

### Generation of bone marrow chimeras

For the generation of bone marrow chimeras, donor-derived bone marrow cells from *Cd23*-Cre *Ikzf1* $^{fl/-}$ Eβ$^{-/-}$ or *Cd23*-Cre *Ikzf1* $^{fl/+}$ Eβ$^{-/-}$ mice were transferred intravenously into sub-lethally irradiated (5 Gy) *Rag2* $^{-/-}$, $J_HT$ or OT-II TCR-tg *Rag2* $^{-/-}$ recipients. For the generation of mixed bone marrow chimeras, donor-derived bone marrow cells of the indicated genotypes ($CD45.2^+$) were mixed 1:1 with bone marrow cells from $CD45.1^+$ wild-type (WT) mice and transferred intravenously into sub-lethally (5 Gy) irradiated *Rag2* $^{-/-}$ recipients. The mice were analyzed 4-10 weeks after bone marrow reconstitution.

### *In vivo* depletion of $CD4^+$ and $CD8^+$ T cells in *Cd23*- Cre *Ikzf1* $^{fl/fl}$ mice

To deplete $CD4^+$ or $CD8^+$ T cells in experimental *Ikzf1* $^{B-}$ and control *Ikzf1* $^{B+}$ mice before and during the appearance of Ikaros-deficient B cells in peripheral lymphoid organs, we generated bone marrow chimeras by injecting lethally (10 Gy) irradiated wild-type (C57BL/6) or sub-lethally (5 Gy) irradiated $J_HT$ host mice. T cell depletion was initiated by i.p. injection of 50 μg of an anti-CD4 (GK1.5) or anti-CD8 (2.43) antibody one day before ($J_HT$ host) or one day after (wild-type host) the transfer of *Ikzf1* $^{B-}$ or control *Ikzf1* $^{B+}$ bone marrow. These mice were subsequently injected with 50 μg of the in-house produced and purified antibodies at 4-7-day intervals, and the deletion of $CD4^+$ or $CD8^+$ T cells was monitored by flow cytometric analysis of the blood.

### Intracellular flow staining of Ikaros and signaling molecules

Ikaros staining was performed after fixation-permeabilization with the Foxp3 staining buffer set (eBioscience). Analysis of phosphorylated BCR signaling components was performed with mature $CD43^-$ B cells from lymph nodes, which were enriched by immunomagnetic depletion with CD43-MicroBeads (Milteny Biotec), followed by resuspension in RPMI-1640 medium (Gibco) and stimulation for 5 min at 37 °C with 10 μg/ml anti-mouse IgM (II/41) or for indicated time points with 1 μg/ml CpG oligodeoxynucleotides

(ODN1826, InvivoGen). The stimulated cells were mixed with an equal volume of Fixation buffer (BD Cytofix) and fixed for 15 min at 37 °C. Cells were washed with Perm/Wash Buffer I (BD Phosflow) and stained in this buffer with antibodies detecting phosphorylated BCR signaling components or IκBα for at least 1 h at 23 °C at the dilution recommended by the manufacturer. The Ikaros-, IκBα- and phospho-specific antibodies used are described under 'Antibodies'.

### Calcium fluorimetry

Mature CD43$^-$ B cells ($2 \times 10^6$) from the lymph nodes were loaded with the calcium-sensor dye eFluor 514 (eBioscience) at a final concentration of 1 μM in 1 ml of IMDM medium containing 10% fetal calf serum, 1 mM glutamine, 50 μM β-mercaptoethanol. After incubation for 45 min at 37 °C, the cells were washed twice and the fluorescence emission at 530/30 nm (excitation at 488 nm) was measured in live cells on a Fortessa flow cytometer. The acquisition of data was initiated 20 s before the addition of the anti-IgM antibody (II/41) at a concentration of 0.1-1 μg/ml or the antigen HEL (Sigmal/Roche) at a concentration of 3-10 μg/ml. Data were collected for 130 s. The data were analyzed with FlowJo software. The percentage of fluorescent increase ($\Delta F/F_0$) is plotted against time (t) after stimulation (Fig. 5a,c,e). $F_0$ refers to the average fluorescence determined between 0 and 20 sec prior to antibody or antigen addition, and ΔF corresponds to the fluorescence F(t) (measured at time 't') minus $F_0$.

### *In vitro* B cell stimulation experiments

CD43$^-$ FO B cells were enriched from lymph nodes by immunomagnetic depletion of non-B cells with CD43-MicroBeads (Miltenyi Biotec). The sorted cells were labeled with 5 μM CellTrace™ Violet dye (Thermo Fisher Scientific) in PBS for 20 min at 37 °C. After washing with stimulation medium (RPMI-1640 supplemented with 10% heat-inactivated FCS, 1 mM glutamine and 50 μM β-mercaptoethanol), the cells were seeded at a density of $0.5 \times 10^6$ cells in 1 ml of stimulation medium containing 1.3 μg/ml anti-IgM antibody (II/41) plus 10 ng/ml IL-4 or 1.5 μg/ml anti-CD40 (HM40-3, eBioscience), 1 μg/ml HEL (Sigma/Roche), 1 μg/ml (0.2 μM) CpG oligodeoxynucleotides (ODN1826, InvivoGen), 2 μg/ml Pam3 (Pam3CSK4, Invivogen), 1 μg/ml Resiquimod (R848, Invivogen) or 25 μg/ml LPS. At day 4, the proliferation of the stimulated B cells was assessed by flow cytometric analysis. Live/dead separation for in vitro cultured cells was achieved by staining with fixable viability dye eFluor780 (Thermo Fisher Scientific).

### *In vitro* B cell stimulation with the SCHIC reagent

To simultaneously stimulate monoclonal MD4 BCR-tg B cells via the BCR and TLR9 pathways[32], we generated the stimulatory CpG-HEL immune complex (SCHIC) by mixing biotinylated HEL (lysozyme biotin-caproyl (Sigma; L0289), containing 1-2 biotin per protein) and biotinylated CpG oligodeoxynucleotides (ODN 1826 Biotin, InvivoGen) at equal molar ratio prior to the addition of an equimolar amount of strepavidin (SA, Thermo Fisher Scientific). After incubation for 10 min, potentially free CpG-Bio or HEL-Bio molecules were quenched by the further addition of an equal amount of streptavidin. CellTrace Violet-labeled B cells were stimulated with 0.2 μM of this SCHIC reagent and analyzed, as described under '*In vitro* B cell stimulation experiments'.

### Antigen presentation assay

To evaluate the antigen presentation activity of B cells, $CD23^+$ FO and $CD21^{lo/-}CD23^-$ B cells were sorted by flow cytometry as $CD19^+B220^{hi}CD138^-CD93^-CD21^{int}CD23^+$ or $CD19^+B220^{hi}CD138^-CD93^-CD21^{lo/-}CD23^-$ cells, respectively. The purified B cells were resuspended in medium at a concentration of $2 \times 10^6$ cells/ml. Either 2 μg/ml OT-II (Ovalbumin 323-339, InvivoGen) or 2 μg/ml OT-I peptide (Ovalbumin 257-264) was added and incubated for 20 min at 37 °C and subsequently washed 3 times with complete RPMI medium to remove excess free peptides. OT-II T cells were purified from the spleen and lymph nodes of OT-II TCR-tg *Rag2*$^{-/-}$ mice by staining myeloid cells with CD115-Bio, CD11c-Bio and CD11b-Bio followed by their depletion with anti-biotin-MicroBeads (Miltenyi Biotec). The purified OT-II T cells were labeled with 5 μM CellTrace Violet dye (Thermo Fisher Scientific) in PBS for 20 min at 37 °C. Peptide-loaded FO B cells and CellTrace Violet-labeled $CD4^+$ T cells were co-cultured at a 1:1 ratio (50,000 cells of each cell type) in a 96-well V bottom plate, and T cell proliferation as well as activation was analyzed after 4 days by flow cytometry.

### HEL injection

For *in vivo* HEL exposure of monoclonal MD4 BCR-tg B cells, 200 μg of HEL (Sigma/Roche) in PBS was injected i.v. into MD4 BCR-tg *Ikzf1*$^{B-}$ and MD4 BCR-tg *Ikzf1*$^{B+}$ mice.

### Immunization

The immune response to a T cell-dependent antigen was studied by intraperitoneal injection of 100 μg of 4-hydroxy-3-nitrophenylacetyl-conjugated keyhole limpet hemocyanin (NP-KLH; Biosearch Technologies) in alum. Germinal center and plasma cell development was studied after 9-14 days by flow cytometry and immunohistology.

### Serum concentration of cytokine and antibody isotypes

Concentrations of cytokines in serum (Supplementary Fig. 2b) were analyzed with the multiplex, bead-based technology (ProcartaPlex, eBioscience) using a custom 15-Plex kit for testing the following factors: IFN-γ, TNF, G-CSF, GM-CSF, M-CSF, IL-1α, IL-1β, IL-3, IL-6, IL-7, IL-10, IL-17A IL-12p70, IL-23 and IL-27. The serum titer of various antibody isotypes (Supplementary Fig. 2h) was measured using Procarta Isotyping Panel 1 Multiplex kit (ProcartaPlex Isotyping 7-Plex, eBioscience). Data were acquired and analyzed by Bioplex (Bio-Rad).

### Immunohistochemical analysis

Spleens were fixed in PBS with 4% paraformaldehyde for 1 h and cryoprotected in PBS plus 30% sucrose for > 3 h to overnight before being embedded in optimum cutting temperature compound (OCT) and frozen. Frozen spleens were sectioned (5-10 μm) and fixed in acetone. For immunostaining, all incubations were performed in a humidified chamber at room temperature. Sections were blocked in 5% BSA. Antibodies (described in the ‘Antibodies’ section), PNA-Bio (Vector Laboratories), SA-Cy3 (Jackson ImmunoResearch Laboratories) and SA-Alexa647 (Jackson ImmunoResearch Laboratories) were used for staining. One day after mounting with ProLong Gold Antifade Mountant (Molecular Probes), confocal images

were acquired on an LSM780 Axio Imager Z2 system (Zeiss). *z*-stacks and arrays of images were obtained with a Plan-Apochromat 25x (NA 0.8, Imm corr) objective and motorized stage.

### Indirect immunofluorescence assay using HEp-2 slides

Diluted mouse serum (1:100 in PBS) was incubated on HEp-2 slides (Orgentech) for 30 min in the dark at 22 ºC using a humidity chamber. Subsequently, the slides were rinsed once with a squirt bottle and washed twice for 5 min with PBS. For detection of mouse IgG, the slides were incubated for 30 min in the dark at 22 ºC in a humidity chamber with an Alexa488-conjugated goat anti-mouse IgG (H+L) antibody (Thermo Fisher Scientific) as a secondary antibody. Following two washing steps, DAPI-containing mounting medium (Life Technologies) was added together with a cover slip. Images were acquired with a Panoramic slide scanner.

### Histopathological analysis

For histopathological analyses, the liver, kidney, pancreas, lung, thymus, cervical lymph nodes, and spleen of 8- and 10-week-old *Ikzf1* $^{B-}$ and *Ikzf1* $^{B+}$ mice were fixed in 4% paraformaldehyde and then processed for immunohistochemical analysis by staining sections with hematoxylin and eosin (H&E) as well as with anti-B220 and anti-CD3 antibodies. Stained slides were reviewed by a board-certified pathologist with a Zeiss Axioskop 2 MOT microscope (Carl Zeiss Microscopy).

### Immunoblot analysis of TNFAIP3 expression in CpG- and R848-stimulated B cells

*In vitro* stimulated B cells (see section '*In vitro* B cell stimulation experiments') were pelleted and snap-frozen in liquid nitrogen. Cells were lysed in 4% SDS, 120 mM Tris (pH 6.8) buffer ($10^6$ cells in 50 µl lysis buffer). After adding 3× SDS sample buffer, cell lysates were separated by SDS-PAGE, followed by immunoblot analysis. TNFAIP3 (A20) was detected with a monoclonal rabbit antibody (D13H3, Cell Signaling) and an HRP-conjugated anti-rabbit secondary antibody (Sigma/GE Healthcare). GAPDH, which was detected with the HRP-conjugated monoclonal rabbit antibody 14C10 (Cell Signaling), was used as loading control.

### Bio-ChIP-seq analysis of Ikaros binding

Chromatin of $1 \times 10^8$ naïve CD43$^-$ or CD23$^+$ splenic B cells isolated from *Ikzf1* $^{ihCd2/ihCD2}$ *Rosa26* $^{BirA/BirA}$ mice[19] was subjected to cross-linking at room temperature for 10 min with 1% formaldehyde followed by nuclei isolation and lysate preparation. Optionally, the chromatin was prepared using 8 M urea density gradient ultra-centrifugation[58]. Following DNA shearing by using the Bioruptor sonicator (Diagenode), Ikaros-bound DNA was immunoprecipitated using Streptavidin Mag Sepharose (GE Healthcare). The ChIP-precipitated DNA (1–2 ng) was used for library preparation and subsequent Illumina deep sequencing (Table 6).

### Mapping of open chromatin regions

Open chromatin regions were mapped in FO B cells and CpG-stimulated B cells by the ATAC-seq method as described[59] with the modification that the nuclei were prepared by incubating cells with nuclear preparation buffer (0.3 M sucrose, 10 mM Tris pH 7.5, 60 mM KCl, 15 mM NaCl, 5 mM $MgCl_2$, 0.1 mM EGTA, 0.1% NP-40, 0.15 mM spermine, 0.5 mM spermidine, and 2 mM 6AA) before treatment with the transposase Tn5 (4 μl of Nextera Tn5 transposase per 20,000 cells).

### cDNA preparation for RNA-seq

Total RNA from *ex vivo* sorted or *in vitro* stimulated FO B cells was isolated with the RNeasy Plus Mini Kit (Qiagen), and mRNA was purified by two rounds of poly(A) selection with the Dynabeads mRNA purification kit (Invitrogen). The mRNA was fragmented by heating at 94 °C for 3 min in fragmentation buffer. The fragmented mRNA was used as template for first-strand cDNA synthesis with random hexamers and the Superscript Vilo First-Strand Synthesis System (Invitrogen). The second-strand cDNA synthesis was performed with 100 mM dATP, dCTP, dGTP and dUTP in the presence of RNase H, *E. coli* DNA polymerase I and DNA ligase (Invitrogen). The incorporation of dUTP allowed for specific elimination of the second DNA strand during library preparation, thereby preserving strand specificity[60].

### Library preparation and Illumina Deep Sequencing

About 1-5 ng of cDNA or ChIP-precipitated DNA was used as starting material for the generation of sequencing libraries with the NEBNext Ultra Ligation Module and NEBNext End Repair/dA-Tailing module. DNA fragments of the following sizes were selected: 200–500 bp for ChIP-seq and 150–700 bp for RNA-seq with AMPure XP beads (Beckman Coulter). For strand-specific RNA-seq, the uridines present in one cDNA strand were digested with uracil-N-glycosylase (New England BioLabs) as described[60], followed by PCR amplification with the KAPA Real Time Amplification kit (KAPA Biosystems). Completed libraries were quantified with the Bioanalyzer dsDNA 1000 assay kit (Agilent) and QPCR NGS Library Quantification kit (Agilent). Cluster generation and sequencing were carried out by using the Illumina HiSeq 2500 system with 50 nucleotides read length, according to the manufacturer's guidelines.

### Database of RefSeq-annotated genes

The database generation of RefSeq-annotated genes was performed as previously described[61]. To refine the annotation of immunoglobulin genes, the immunoglobulin λ light-chain segments were replaced with their corresponding converted GRCm38.p3 annotations (Ensembl version 79)[62]. The resulting number of genes was 24,732.

### Sequence alignment

In case of RNA-seq experiments, reads corresponding to mouse ribosomal RNAs (BK000964.1 and NR046144.1) were removed. The remaining reads were cut down to a read length of 44 nucleotides and aligned to the mouse transcriptome (genome assembly version of July 2007 NCBI37/mm9) using TopHat version 1.4.1 (ref. 63). In case of ChIP-

seq and ATAC-seq experiments, all sequence reads that passed the Illumina quality filtering were considered for alignment after adapter trimming. The remaining reads were aligned to the mouse genome assembly version of July 2007 (NCBI37/mm9), using the Bowtie program versions 0.12.1 and 2.1.0, respectively[64]. For ATAC-seq, additional alignment parameters were '-sensitive -X 5000'.

### Peak calling

After alignment, the datasets of all four Ikaros Bio-ChIP-seq experiments have been converted to bigWig format and normalized to reads per million using samtools 1.4 (ref. 65) and UCSC kent tools[66]. The files have been subsequently merged into one track using deeptools 3.0.1 (ref. 67) with the bigwigCompare commands. Ikaros peaks were called with a *P* value of $< 10^{-10}$ by using the MACS program version 2.1.0 (ref. 68) with default parameters, the input control of mature B cells (GSM2058441) and a genome size of 1,870,000,000 bp.

### Peak-to-gene assignment

Ikaros target genes were identified by peak-to-gene assignment as described[69]. Peaks were assigned to genes in a stepwise manner by prioritizing genes containing peaks in their promoter and/or gene body. For this, peaks overlapping with the promoter (-2.5 kb to +2.5 kb relative to TSS) or gene body (+2.5 kb to TES) were first assigned to the corresponding gene. Other peaks within a specified region of 50 kb upstream of the TSS or downstream of the TES were assigned to the gene containing peaks in the promoter or gene body. All other peaks within the same specified region were assigned to the nearest gene, and all non-assigned peaks were classified as intergenic.

### Analysis of RNA-seq data

The number of reads per gene was counted using featureCounts version 1.5.0 (ref. 70) with default settings. TPM values were calculated as described[71]. For analyzing the differential gene expression of non-stimulated, 1 day *in vivo* HEL-exposed or 1 day *in vitro* CpG-stimulated FO B cells of MD4 BCR-tg *Ikzf1* $^{B-}$ and MD4 BCR-tg *Ikzf1* $^{B+}$ mice or anergic FO B cells of MD4 BCR-tg ML5-tg mice, the datasets were separated in individual groups according to genotype, sequencing batch and stimulation. The groups were subsequently analyzed together using the R package DESeq2 version 1.18.1 (ref. 72). Sample normalizations and dispersion estimations were conducted using the default DESeq2 settings. Wald tests were performed with the model design formula "~ group" (which is a linear combination of genotype, sequencing batch, and stimulation), each *Ikzf1* $^{B-}$ group was compared to its corresponding *Ikzf1* $^{B+}$ stimulation within the same sequencing batch. Regularized log transformations were computed with the blind option set to 'FALSE' and were transformed from $\log_2$ to $\log_{10}$ scale for the scatterplots shown in Fig. 7b and Supplementary Fig. 6c,d. Genes with an adjusted *P* value < 0.05, TPM (averaged within groups) > 5 at least in one group, and a fold-change of > 2 or > 3 for the Ikaros- or anergy-dependent datasets, respectively, were called as significantly expressed. A combined dataset of Ikaros-regulated genes in FO B cells was defined by combining regulated genes from naïve and HEL-exposed FO B cells (Supplementary Fig. 6c,d) and selected for an adjusted *P* value of < 0.05 in HEL-exposed FO B cells. By applying a cutoff of > 2-fold for the

summed fold-change, genes regulated in opposite directions in naïve and HEL-exposed FO B cells were eliminated. Except for the mRNAs encoding the MD4 BCR, all transcripts of the V, D and J gene segments at the *Igh*, *Igk* and *Igl* loci were eliminated from the list of significantly regulated genes in the anergy gene signature dataset, although the immunoglobulin and T cell receptor transcripts were included in all TPM calculations.

### Statistical analysis

Statistical analysis was performed with the GraphPad Prism 7 software. Unpaired, two-tailed Student's *t*-test analysis was used to assess the statistical significance of one observed parameter between two experimental groups. If more than one parameter (age, cell subsets) were measured in two experimental groups, multiple *t*-tests (unpaired, two-tailed) were applied, and the Holm-Sidac multi comparison test was used to report the significance between the two groups. One-way ANOVA was used when more than two experimental groups were compared, and the statistical significance was determined by Tukey post hoc test. The statistical evaluation of the RNA-seq data is described under 'Analysis of RNA-seq data'.

## Supplementary Material

Refer to Web version on PubMed Central for supplementary material.

## Acknowledgements

We thank R. Medzhitov, A. Tarakhovsky and S.L. Nutt for providing *Myd88* $^{fl/fl}$, *Prdm1* $^{fl/fl}$ and *Prdm1* $^{Gfp/+}$ mice, respectively, J. Cyster for providing the HyHEL9 antibody, G. Schmauß and M. Weninger for FACS sorting, A. Sommer's team at the Vienna Biocenter Support Facilities GmbH (VBCF) for Illumina sequencing and A. Kavirayani's team at VBCF for histology support and pathology review. This research was supported by Boehringer Ingelheim, the European Research Council (ERC) under the European Union's Horizon 2020 research and innovation program (grant agreement No 740349-PlasmaCellControl), the Austrian Industrial Research Promotion Agency (Headquarter Grant FFG-852936) and the Austrian Science Fund (T838-B26 to T.A.S.).

## References

1. Nutt SL, Hodgkin PD, Tarlinton DM, Corcoran LM. The generation of antibody-secreting plasma cells. Nat Rev Immunol. 2015; 15:160–171. [PubMed: 25698678]
2. Wardemann H, et al. Predominant autoantibody production by early human B cell precursors. Science. 2003; 301:1374–1377. [PubMed: 12920303]
3. Zikherman J, Parameswaran R, Weiss A. Endogenous antigen tunes the responsiveness of naïve B cells but not T cells. Nature. 2012; 489:160–164. [PubMed: 22902503]
4. Theofilopoulos AN, Kono DH, Baccala R. The multiple pathways to autoimmunity. Nat Immunol. 2017; 18:716–724. [PubMed: 28632714]
5. Cambier JC, Gauld SB, Merrell KT, Vilen BJ. B-cell anergy: from transgenic models to naturally occurring anergic B cells? Nat Rev Immunol. 2007; 7:633–643. [PubMed: 17641666]
6. Rawlings DJ, Metzler G, Wray-Dutra M, Jackson SW. Altered B cell signalling in autoimmunity. Nat Rev Immunol. 2017; 17:421–436. [PubMed: 28393923]
7. Tsokos GC, Lo MS, Costa Reis P, Sullivan KE. New insights into the immunopathogenesis of systemic lupus erythematosus. Nat Rev Rheumatol. 2016; 12:716–730. [PubMed: 27872476]
8. Georgopoulos K. The making of a lymphocyte: the choice among disparate cell fates and the IKAROS enigma. Genes Dev. 2017; 31:439–450. [PubMed: 28385788]

9. Han J-W, et al. Genome-wide association study in a Chinese Han population identifies nine new susceptibility loci for systemic lupus erythematosus. Nat Genet. 2009; 41:1234–1237. [PubMed: 19838193]
10. Gateva V, et al. A large-scale replication study identifies *TNIP1, PRDM1, JAZF1, UHRF1BP1* and *IL10* as risk loci for systemic lupus erythematosus. Nat Genet. 2009; 41:1228–1233. [PubMed: 19838195]
11. He CF, et al. TNIP1, SLC15A4, ETS1, RasGRP3 and IKZF1 are associated with clinical features of systemic lupus erythematosus in a Chinese Han population. Lupus. 2010; 19:1181–1186. [PubMed: 20516000]
12. Cunninghame Graham DS, et al. Association of *NCF2, IKZF1, IRF8, IFIH1* and *TYK2* with systemic lupus erythematosus. PLoS Genet. 2011; 7:e1002341. [PubMed: 22046141]
13. Farh KK-H, et al. Genetic and epigenetic fine mapping of causal autoimmune disease variants. Nature. 2015; 518:337–343. [PubMed: 25363779]
14. Zhang Y-M, et al. Association of the *IKZF1* 5' UTR variant rs1456896 with lupus nephritis in a northern Han Chinese population. Scand J Rheumatol. 2017; 46:210–214. [PubMed: 27684961]
15. Kuehn HS, et al. Loss of B cells in patients with heterozygous mutations in IKAROS. N Engl J Med. 2016; 374:1032–1043. [PubMed: 26981933]
16. Hoshino A, et al. Abnormal hematopoiesis and autoimmunity in human subjects with germline *IKZF1* mutations. J Allergy Clin Immunol. 2017; 140:223–231. [PubMed: 27939403]
17. Bogaert DJ, et al. A novel IKAROS haploinsufficiency kindred with unexpectedly late and variable B-cell maturation defects. J Allergy Clin Immunol. 2018; 141:432–435. [PubMed: 28927821]
18. Van Nieuwenhove E, et al. A kindred with mutant IKAROS and autoimmunity. J Allergy Clin Immunol. 2018; 142:699–702. [PubMed: 29705243]
19. Schwickert TA, et al. Stage-specific control of early B cell development by the transcription factor Ikaros. Nat Immunol. 2014; 15:283–293. [PubMed: 24509509]
20. Kwon K, et al. Instructive role of the transcription factor E2A in early B lymphopoiesis and germinal center B cell development. Immunity. 2008; 28:751–762. [PubMed: 18538592]
21. Naradikian MS, Hao Y, Cancro MP. Age-associated B cells: key mediators of both protective and autoreactive humoral responses. Immunol Rev. 2016; 269:118–129. [PubMed: 26683149]
22. Rubtsova K, Rubtsov AV, Cancro MP, Marrack P. Age-associated B cells: a T-bet-dependent effector with roles in protective and pathogenic immunity. J Immunol. 2015; 195:1933–1937. [PubMed: 26297793]
23. Kallies A, Xin A, Belz GT, Nutt SL. Blimp-1 transcription factor is required for the differentiation of effector $CD8^+$ T cells and memory responses. Immunity. 2009; 31:283–295. [PubMed: 19664942]
24. Gu H, Zou YR, Rajewsky K. Independent control of immunoglobulin switch recombination at individual switch regions evidenced through Cre-*loxP*-mediated gene targeting. Cell. 1993; 73:1155–1164. [PubMed: 8513499]
25. Goodnow CC, et al. Altered immunoglobulin expression and functional silencing of self-reactive B lymphocytes in transgenic mice. Nature. 1988; 334:676–682. [PubMed: 3261841]
26. Goodnow CC, Crosbie J, Jorgensen H, Brink RA, Basten A. Induction of self-tolerance in mature peripheral B lymphocytes. Nature. 1989; 342:385–391. [PubMed: 2586609]
27. Sabouri Z, et al. IgD attenuates the IgM-induced anergy response in transitional and mature B cells. Nat Commun. 2016; 7
28. Enders A, et al. Zinc-finger protein ZFP318 is essential for expression of IgD, the alternatively spliced Igh product made by mature B lymphocytes. Proc Natl Acad Sci USA. 2014; 111:4513–4518. [PubMed: 24616512]
29. Pioli PD, Debnath I, Weis JJ, Weis JH. Zfp318 regulates IgD expression by abrogating transcription termination within the *Ighm/Ighd* locus. J Immunol. 2014; 193:2546–2553. [PubMed: 25057009]
30. Sharma S, Fitzgerald KA, Cancro MP, Marshak-Rothstein A. Nucleic acid-sensing reeceptors: rheostats of autoimmunity and autoinflammation. J Immunol. 2015; 195:3507–3512. [PubMed: 26432899]

31. Nickerson KM, et al. TLR9 promotes tolerance by restricting survival of anergic anti-DNA B cells, yet is also required for their activation. J Immunol. 2013; 190:1447–1456. [PubMed: 23296704]
32. Sindhava VJ, et al. A TLR9-dependent checkpoint governs B cell responses to DNA-containing antigens. J Clin Invest. 2017; 127:1651–1663. [PubMed: 28346226]
33. Kobayashi K, et al. IRAK-M is a negative regulator of Toll-like receptor signaling. Cell. 2002; 110:191–202. [PubMed: 12150927]
34. Tavares RM, et al. The ubiquitin modifying enzyme A20 restricts B cell survival and prevents autoimmunity. Immunity. 2010; 33:181–191. [PubMed: 20705491]
35. Chu Y, et al. B cells lacking the tumor suppressor TNFAIP3/A20 display impaired differentiation and hyperactivation and cause inflammation and autoimmunity in aged mice. Blood. 2011; 117:2227–2236. [PubMed: 21088135]
36. Abdul-Sater AA, et al. The signaling adaptor TRAF1 negatively regulates Toll-like receptor signaling and this underlies its role in rheumatic disease. Nat Immunol. 2017; 18:26–35. [PubMed: 27893701]
37. Schenten D, et al. Signaling through the adaptor molecule MyD88 in $CD4^+$ T cells is required to overcome suppression by regulatory T cells. Immunity. 2014; 40:78–90. [PubMed: 24439266]
38. Shin H, et al. A role for the transcriptional repressor Blimp-1 in $CD8^+$ T cell exhaustion during chronic viral infection. Immunity. 2009; 31:309–320. [PubMed: 19664943]
39. Hale JS, Boursalian TE, Turk GL, Fink PJ. Thymic output in aged mice. Proc Natl Acad Sci USA. 2006; 103:8447–8452. [PubMed: 16717190]
40. Chan OT, Hannum LG, Haberman AM, Madaio MP, Shlomchik MJ. A novel mouse with B cells but lacking serum antibody reveals an antibody-independent role for B cells in murine lupus. J Exp Med. 1999; 189:1639–1648. [PubMed: 10330443]
41. Amano H, et al. The *Yaa* mutation promoting murine lupus causes defective development of marginal zone B cells. J Immunol. 2003; 170:2293–2301. [PubMed: 12594250]
42. Degn SE, et al. Clonal evolution of autoreactive germinal centers. Cell. 2017; 170:913–926. [PubMed: 28841417]
43. Noviski M, et al. IgM and IgD B cell receptors differentially respond to endogenous antigens and control B cell fate. eLife. 2018; 7:e35074. [PubMed: 29521626]
44. Übelhart R, et al. Responsiveness of B cells is regulated by the hinge region of IgD. Nat Immunol. 2015; 16:534–543. [PubMed: 25848865]
45. Maity PC, et al. B cell antigen receptors of the IgM and IgD classes are clustered in different protein islands that are altered during B cell activation. Sci Signal. 2015; 8:ra93. [PubMed: 26373673]
46. Noviski M, Zikherman J. Control of autoreactive B cells by IgM and IgD B cell receptors: maintaining a fine balance. Curr Opin Immunol. 2018; 55:67–74. [PubMed: 30292928]
47. Sun H, Lu B, Li R-Q, Flavell RA, Taneja R. Defective T cell activation and autoimmune disorder in Stra13-deficient mice. Nat Immunol. 2001; 2:1040–1047. [PubMed: 11668339]
48. Li S, et al. The transcription factors Egr2 and Egr3 are essential for the control of inflammation and antigen-induced proliferation of B and T cells. Immunity. 2012; 37:685–696. [PubMed: 23021953]
49. Lech M, et al. Interleukin-1 receptor-associated kinase-M suppresses systemic lupus erythematosus. Ann Rheum Dis. 2011; 70:2207–2217. [PubMed: 21875872]
50. Shlomchik MJ, Madaio MP, Ni D, Trounstein M, Huszar D. The role of B cells in *lpr*/*lpr*-induced autoimmunity. J Exp Med. 1994; 180:1295–1306. [PubMed: 7931063]
51. Wang J-H, et al. Selective defects in the development of the fetal and adult lymphoid system in mice with an Ikaros null mutation. Immunity. 1996; 5:537–549. [PubMed: 8986714]
52. Kallies A, et al. Plasma cell ontogeny defined by quantitative changes in Blimp-1 expression. J Exp Med. 2004; 200:967–977. [PubMed: 15492122]
53. Ohinata Y, et al. Blimp1 is a critical determinant of the germ cell lineage in mice. Nature. 2005; 436:207–213. [PubMed: 15937476]
54. Bouvier G, et al. Deletion of the mouse T-cell receptor b gene enhancer blocks ab T-cell development. Proc Natl Acad Sci USA. 1996; 93:7877–7881. [PubMed: 8755570]

55. Shinkai Y, et al. RAG-2-deficient mice lack mature lymphocytes owing to inability to initiate V(D)J rearrangement. Cell. 1992; 68:855–867. [PubMed: 1547487]
56. Driegen S, et al. A generic tool for biotinylation of tagged proteins in transgenic mice. Transgenic Res. 2005; 14:477–482. [PubMed: 16201414]
57. Barnden MJ, Allison J, Heath WR, Carbone FR. Defective TCR expression in transgenic mice constructed using cDNA-based a- and b-chain genes under the control of heterologous regulatory elements. Immunol Cell Biol. 1998; 76:34–40. [PubMed: 9553774]
58. Kohwi-Shigematsu T, et al. SATB1-mediated functional packaging of chromatin into loops. Methods. 2012; 58:243–254. [PubMed: 22782115]
59. Buenrostro JD, Giresi PG, Zaba LC, Chang HY, Greenleaf WJ. Transposition of native chromatin for fast and sensitive epigenomic profiling of open chromatin, DNA-binding proteins and nucleosome position. Nat Methods. 2013; 10:1213–1218. [PubMed: 24097267]
60. Parkhomchuk D, et al. Transcriptome analysis by strand-specific sequencing of complementary DNA. Nucleic Acids Res. 2009; 37:e123. [PubMed: 19620212]
61. Wöhner M, et al. Molecular functions of the transcription factors E2A and E2-2 in controlling germinal center B cell and plasma cell development. J Exp Med. 2016; 213:1201–1221. [PubMed: 27261530]
62. Yates A, et al. Ensembl 2016. Nucleic Acids Res. 2016; 44:D710–D716. [PubMed: 26687719]
63. Trapnell C, Pachter L, Salzberg SL. TopHat: discovering splice junctions with RNA-Seq. Bioinformatics. 2009; 25:1105–1111. [PubMed: 19289445]
64. Langmead B, Trapnell C, Pop M, Salzberg SL. Ultrafast and memory-efficient alignment of short DNA sequences to the human genome. Genome Biol. 2009; 10:R25. [PubMed: 19261174]
65. Li H, et al. The Sequence Alignment/Map format and SAMtools. Bioinformatics. 2009; 25:2078–2079. [PubMed: 19505943]
66. Kuhn RM, Haussler D, Kent WJ. The UCSC genome browser and associated tools. Brief Bioinform. 2013; 14:144–161. [PubMed: 22908213]
67. Ramírez F, Dündar F, Diehl S, Grüning BA, Manke T. deepTools: a flexible platform for exploring deep-sequencing data. Nucleic Acids Res. 2014; 42:W187–W191. [PubMed: 24799436]
68. Zhang Y, et al. Model-based analysis of ChIP-Seq (MACS). Genome Biol. 2008; 9:R137. [PubMed: 18798982]
69. Revilla-i-Domingo R, et al. The B-cell identity factor Pax5 regulates distinct transcriptional programmes in early and late B lymphopoiesis. EMBO J. 2012; 31:3130–3146. [PubMed: 22669466]
70. Liao Y, Smyth GK, Shi W. featureCounts: an efficient general purpose program for assigning sequence reads to genomic features. Bioinformatics. 2014; 30:923–930. [PubMed: 24227677]
71. Wagner GP, Kin K, Lynch VJ. Measurement of mRNA abundance using RNA-seq data: RPKM measure is inconsistent among samples. Theory Biosci. 2012; 131:281–285. [PubMed: 22872506]
72. Love MI, Huber W, Anders S. Moderated estimation of fold change and dispersion for RNA-seq data with DESeq2. Genome Biol. 2014; 15:550. [PubMed: 25516281]

Europe PMC Funders Author Manuscripts

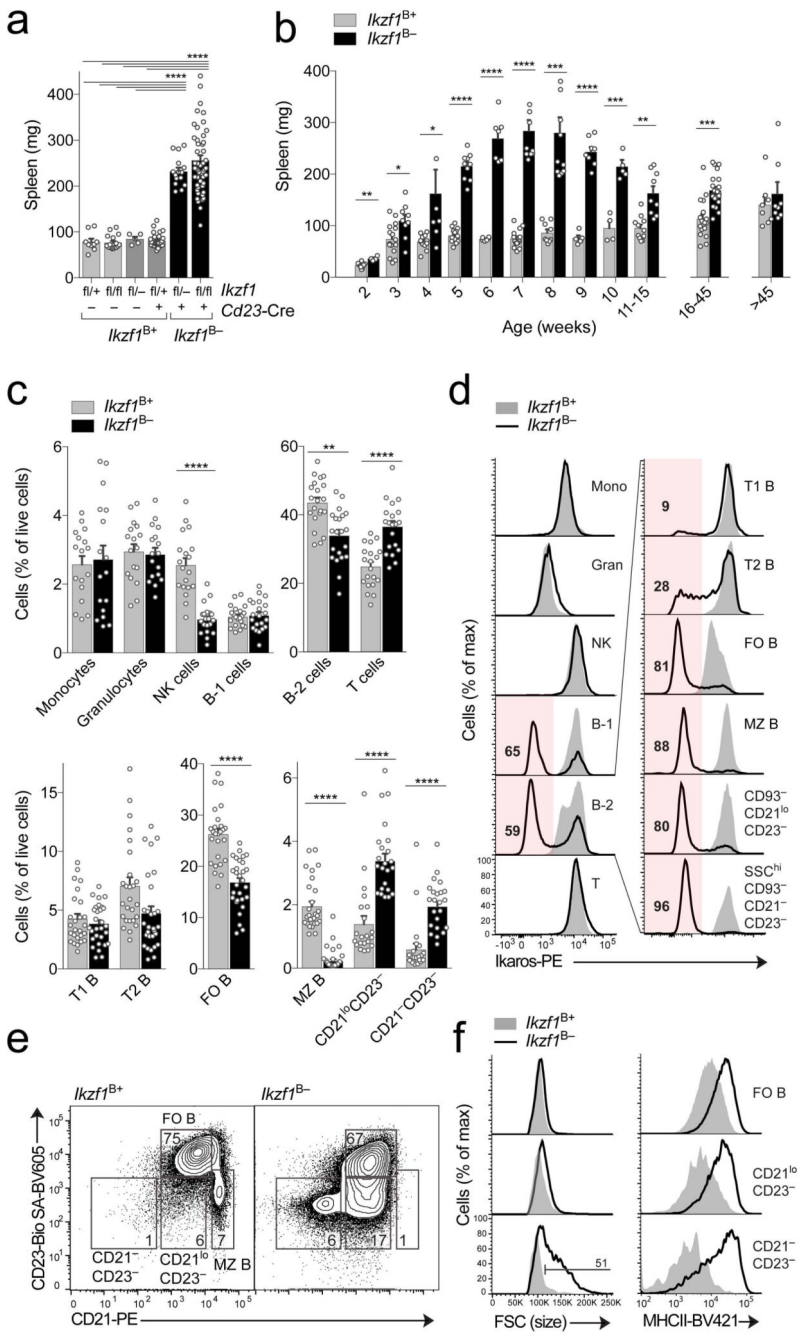


**Fig. 1. Splenomegaly in mice with conditional loss of Ikaros in mature B cells.**

**a**, Increased spleen size upon conditional *Ikzf1* deletion in mature B cells. The weight of the spleen was determined for experimental *Cd23*-Cre *Ikzf1* $^{fl/–}$ ($n$ = 15) and *Cd23*-Cre *Ikzf1* $^{fl/fl}$ ($n$ = 51) mice (collectively referred to as *Ikzf1* $^{B–}$; black) and for control *Ikzf1* $^{fl/fl}$ ($n$ = 17), *Ikzf1* $^{fl/+}$ ($n$ = 9), *Ikzf1* $^{fl/–}$ ($n$ = 5) and *Cd23*-Cre *Ikzf1* $^{fl/+}$ ($n$ = 29) mice (collectively referred to as *Ikzf1* $^{B+}$; gray) at the age of 5-10 weeks. **b**, Age-dependent increase of the spleen size. The weight of the spleen was determined for *Ikzf1* $^{B–}$ (black, $n$ = 4-21) and *Ikzf1* $^{B+}$ (gray, $n$ = 6-17) mice at the indicated ages. **c**, Relative frequencies of different

hematopoietic cell types (upper panel) and B cell subsets (lower panel) among total live cells in the spleen of *Ikzf1* $^{B-}$ (black) and *Ikzf1* $^{B+}$ (gray) mice ($n$ = 17-29), as determined by flow cytometric analysis. **d**, Evaluation of *Ikzf1* deletion through analysis of Ikaros expression by intracellular staining and flow cytometry of the indicated splenic cell types in *Ikzf1* $^{B-}$ (black line) and *Ikzf1* $^{B+}$ (gray) mice. The percentage of Ikaros-deficient cells is indicated. **e**, Flow cytometric analysis of mature splenic B-2 cell subsets ($CD19^+CD5^-CD138^-CD93^-$) in *Ikzf1* $^{B-}$ and *Ikzf1* $^{B+}$ mice. The percentage of cells in each gate is indicated. **f**, Determination of the cell size and expression of the activation marker MHCII by flow cytometric analysis of splenic FO, $CD21^{lo}CD23^-$ and $CD21^-CD23^-$ B cells of the indicated genotypes. Data were obtained in 36 (**a,c**) and 60 (**b**) independent experiments, and data in **d-f** are representative of 20 (**d,e,f** (size)) and 5 (**f** (MHCII)) independent experiments. Mice at the age of 5-10 weeks (**c-f**) were analyzed. Statistical data **(a-c)** are shown as mean values with SEM and were analyzed by one-way ANOVA (Tukey; **a**) or by multiple $t$-tests (unpaired, two-tailed, Holm-Sidac; **b,c**): *$P$ < 0.03, **$P$ < 0.002, ***$P$ < 0.0002, ****$P$ < 0.0001. See Source Data for exact description of the mouse numbers ($n$) and $P$ values. Each dot corresponds to one mouse. The different cell types were defined as described in the Online Methods.

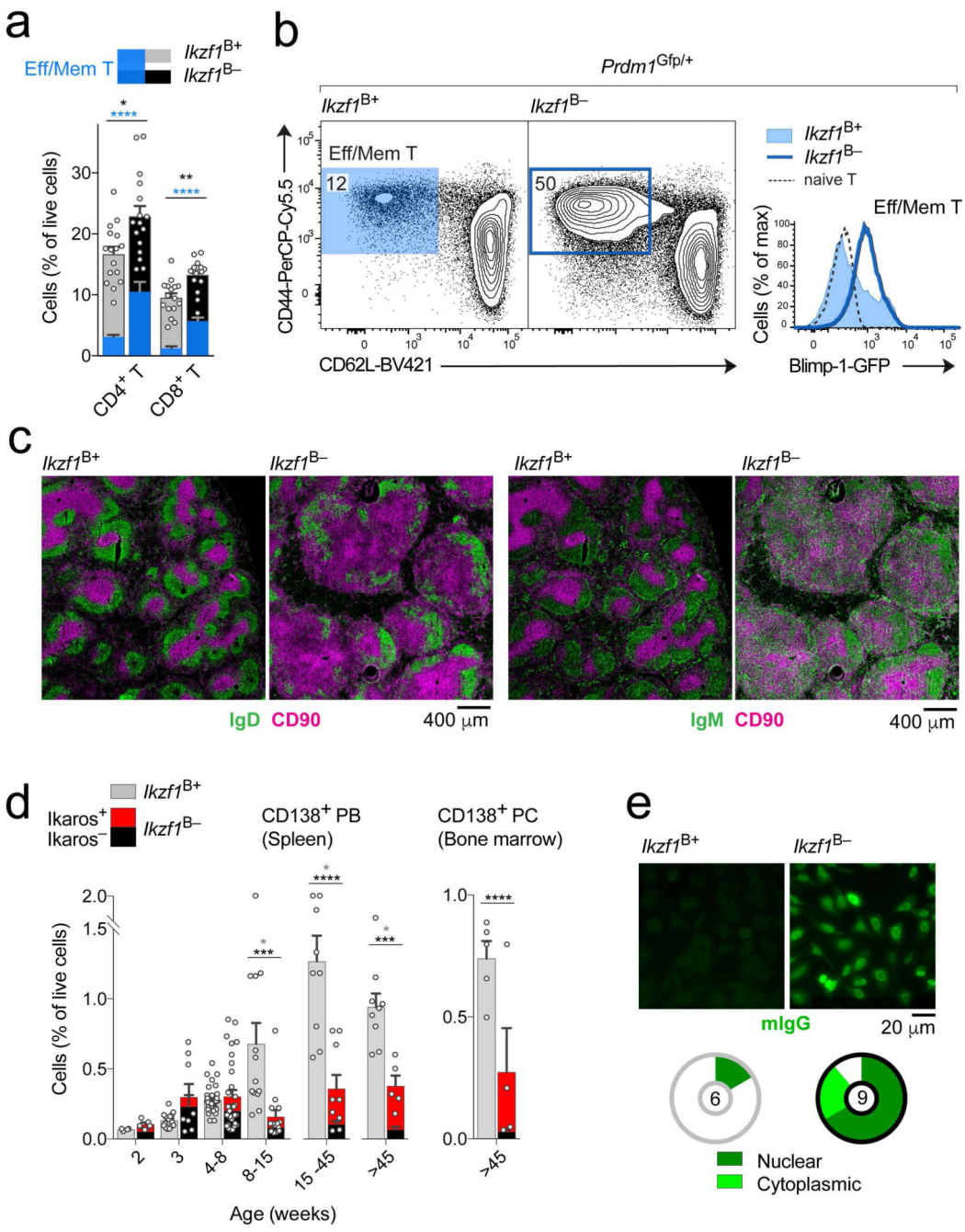


**Fig. 2. Inflammation in the spleen of mice with Ikaros loss in mature B cells.**

**a**, Increase of activated CD44$^{+}$CD62L$^{-}$ T cells in the spleen of *Ikzf1* $^{B-}$ mice. The frequencies of CD4$^{+}$ and CD8$^{+}$ T cells and their activated effector/memory T cell subsets (CD44$^{+}$CD62L$^{-}$; blue shading) among total live cells in the spleen of *Ikzf1* $^{B-}$ (black, $n$ = 16) and *Ikzf1* $^{B+}$ (gray, $n$ = 16) mice were determined by flow cytometry. The statistical significance is indicated for the total (black, gray) and activated (blue) T cell subsets. **b**, Flow cytometric analysis of splenic TCRβ$^{+}$ T cells from *Cd23*-Cre *Ikzf1* $^{fl/fl}$ *Prdm1* $^{Gfp/+}$ (*Ikzf1* $^{B-}$ *Prdm1* $^{Gfp/+}$) and *Cd23*-Cre *Ikzf1* $^{fl/+}$ *Prdm1* $^{Gfp/+}$ (*Ikzf1* $^{B+}$ *Prdm1* $^{Gfp/+}$) mice.




Europe PMC Funders Author Manuscripts

Europe PMC Funders Author Manuscripts

The GFP (Blimp-1) expression of the $CD44^{+}CD62L^{-}$ T cells from the spleen of *Ikzf1* $^{B-}$ *Prdm1* $^{Gfp/+}$ (blue line) or *Ikzf1* $^{B+}$ *Prdm1* $^{Gfp/+}$ (blue shaded) is displayed in the histogram to the right. Naïve wild-type T cells (dashed line) are shown as a negative control. **c**, Immunohistological analysis of the same spleen section from 9-week-old mice of the indicated genotypes. The section was stained with anti-IgD (green, left), anti-IgM (green, right) and anti-CD90 (Thy1.2; purple) antibodies. **d**, The frequencies of $CD138^{+}$ plasmablasts (PB) in the spleen and $CD138^{+}$ plasma cells (PC) in the bone marrow among total live cells of the respective tissue were determined by flow cytometry in *Ikzf1* $^{B-}$ ($n$ = 4-30) and *Ikzf1* $^{B+}$ (gray, $n$ = 4-30) mice at the indicated ages. The PBs and PCs of the *Ikzf1* $^{B-}$ mice were subdivided into *Ikzf1*-deleted (black) and non-deleted (red) cells by intracellular Ikaros staining. The statistical significance of the comparison between *Ikzf1* $^{B+}$ (gray) and non-deleted (red) or *Ikzf1*-deleted (black) PBs and PCs is indicated by gray and black asterisks, respectively. **e**, Representative images of anti-nuclear antibody (ANA) staining obtained with serum from 5-10-week-old *Ikzf1* $^{B-}$ and *Ikzf1* $^{B+}$ mice, as detected by indirect immunofluorescence assay using HEp-2 cells and an Alexa488-conjugated anti-mouse IgG detection antibody (upper panel). The presence of autoreactive IgG antibodies detecting nuclear (dark green) or cytoplasmic (light green) self-antigens was evaluated for 9 *Ikzf1* $^{B-}$ and 6 *Ikzf1* $^{B+}$ mice (lower panel). Data in **a** and **d** were analyzed in 10 and 36 independent experiments, respectively. Data in **b, c** and **e** are representative of 6, 4 and 2 independent experiments, respectively. Statistical data (**a,d)** are shown as mean values with SEM and were analyzed by multiple $t$-tests (unpaired, two-tailed, Holm-Sidac): $*P < 0.03$, $**P < 0.002$, $***P < 0.0002$, $****P < 0.0001$. See Source Data for exact description of the mouse numbers ($n$) and $P$ values. Each dot corresponds to one mouse. The different cell types were defined as described in the Online Methods.

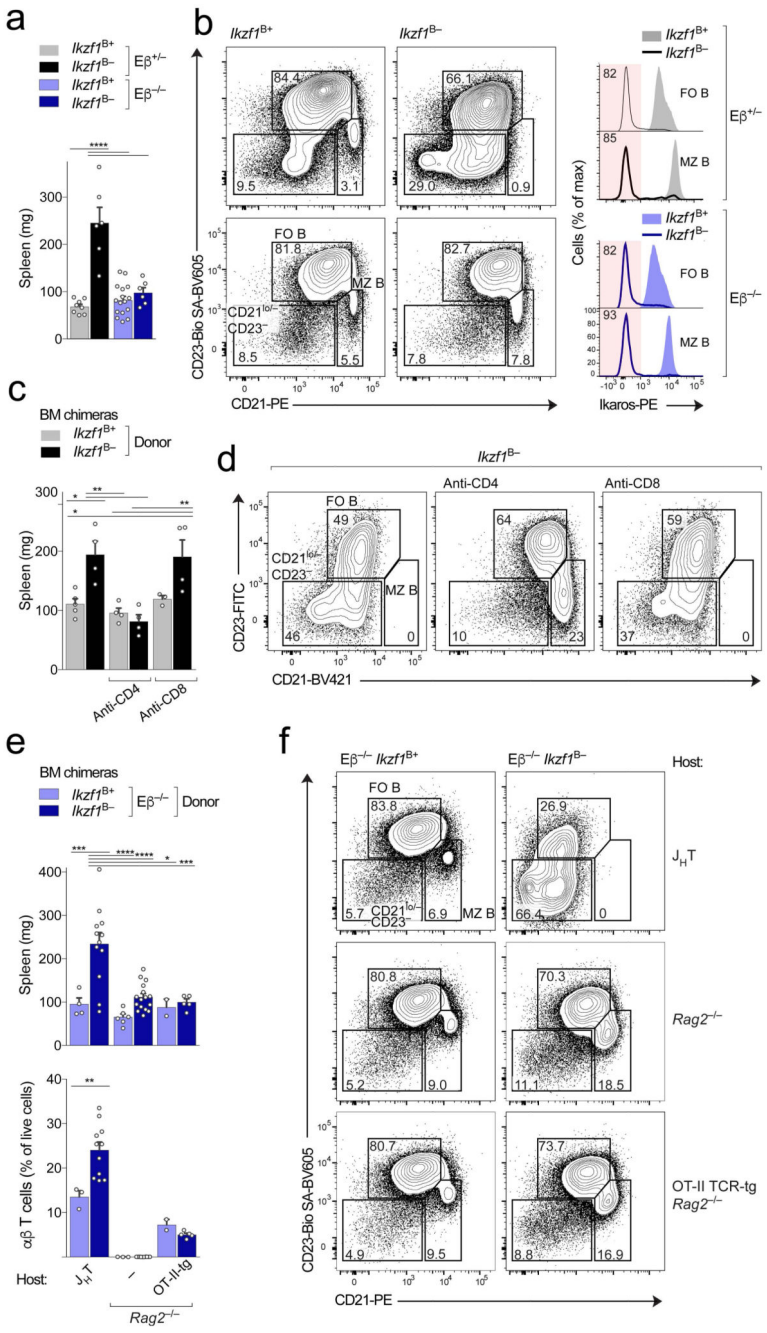


**Fig. 3. Polyclonal T cells contribute to the inflammation in *Ikzf1* $^{B-}$ mice.**

**a**, The spleen weight was determined for Eβ$^{+/-}$ *Ikzf1* $^{B+}$ (gray, $n = 8$), Eβ$^{+/-}$ *Ikzf1* $^{B-}$ (black, $n = 6$), Eβ$^{-/-}$ *Ikzf1* $^{B+}$ (light blue, $n = 16$) and Eβ$^{-/-}$ *Ikzf1* $^{B-}$ (dark blue, $n = 6$) mice at the age of 5-6 weeks. **b**, Flow cytometric analysis of the indicated mature B cell subsets (gated on B-2 cells; CD19$^{+}$CD5$^{-}$CD138$^{-}$CD93$^{-}$) in the spleen of the indicated genotypes (left) and evaluation of the *Ikzf1* deletion frequency in FO and MZ B cells of Eβ$^{+/-}$ *Ikzf1* $^{B-}$ and Eβ$^{-/-}$ *Ikzf1* $^{B-}$ mice by intracellular Ikaros staining (right). The percentage of cells in each gate is indicated. **c,d**, Depletion of CD4$^{+}$ or CD8$^{+}$ T cells. Sub-lethally irradiated $J_HT$ mice were

reconstituted with bone marrow from *Ikzf1* $^{B+}$ (*Ikzf1* $^{+/+}$) or *Ikzf1* $^{B-}$ (*Cd23*-Cre *Ikzf1* $^{fl/fl}$) mice and were then intravenously injected with anti-CD4 ($n$ = 4 or 4) or anti-CD8 ($n$ = 3 or 4) antibodies at regular intervals (after day 1 and week 1, 2, 3 and 4) or kept untreated ($n$ = 5 or 4). At 4.5 or 5 weeks after transplantation, the spleen weight was measured (**c**), and the splenic B and T cells were analyzed by flow cytometry (**d**, gated on B-2 cells), and their frequency was quantified (Supplementary Fig. 3d). **e,f**, Analysis of chimeric mice at 4-5 weeks after transplantation of Eβ$^{-/-}$ *Ikzf1* $^{B+}$ or Eβ$^{-/-}$ *Ikzf1* $^{B-}$ donor bone marrow into sub-lethally irradiated $J_HT$ ($n$ = 4 or 12), *Rag2* $^{-/-}$ ($n$ = 6 or 16) or OT-II TCR-tg *Rag2* $^{-/-}$ ($n$ = 2 or 5) host mice. **e**, The spleen weight is shown for the genetically different chimeras (upper panel), and the frequency of αβ T cells (TCRβ$^{+}$) among total live splenocytes was determined by flow cytometry (lower panel). **f**, Flow cytometric analysis of the indicated mature B cell subsets (gated on B-2 cells) in the spleen of the genetically different chimeras, as described in (**b**). Statistical analysis of the frequencies of the distinct splenic cell types in the different chimeras is shown in Supplementary Fig. 3e. Data in **b, d** and **f** are representative of mice analyzed in **a, c** and **e**, which were examined in 5, 2 and 3 independent experiments, respectively. Statistical data **(a,c,e)** are shown as mean values with SEM and were analyzed by one-way ANOVA (Tukey; **a,c** and **e**, upper panel) or by the unpaired, two-tailed Student's *t*-test (**e**, lower panel): *$P$ < 0.03, **$P$ < 0.002, ***$P$ < 0.0002, ****$P$ < 0.0001. See Source Data for exact description of the mouse numbers ($n$) and $P$ values. Each dot corresponds to one mouse.

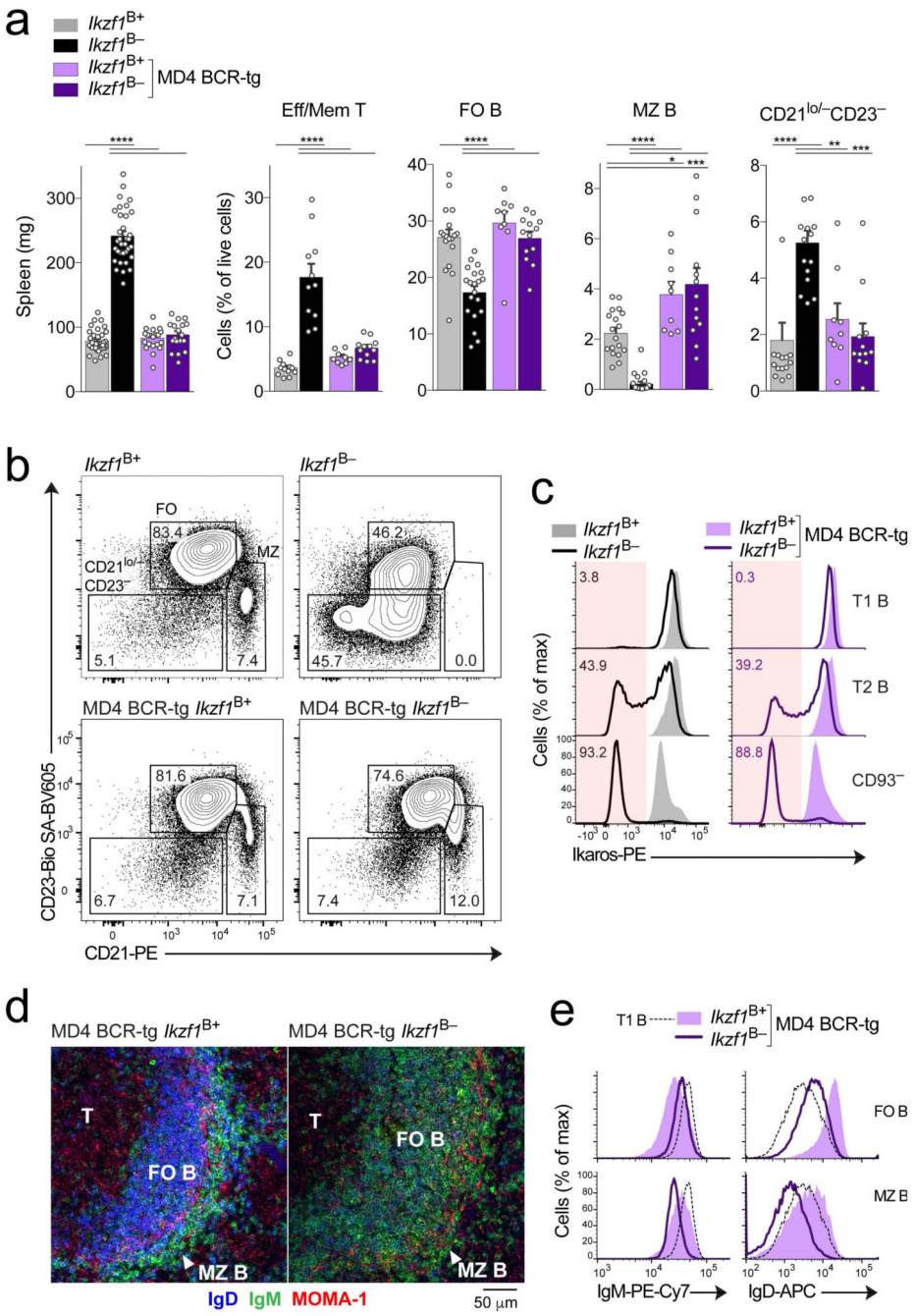


**Fig. 4. Expression of the monoclonal MD4 BCR prevents inflammation in *Ikzf1* $^{B-}$ mice.**

**a**, Determination of the spleen weight and relative abundance of the indicated splenic T and B cell types in *Ikzf1* $^{B+}$ (gray, $n$ = 12-40), *Ikzf1* $^{B-}$ (black, $n$ = 11-34). MD4 BCR-tg *Ikzf1* $^{B+}$ (light purple, $n$ = 9-20) and MD4 BCR-tg *Ikzf1* $^{B-}$ (dark purple, $n$ = 12-18) at the age of 5-10 weeks. The frequency of the different cell types among total live splenocytes was determined by flow cytometry. **b**, Flow cytometric analysis of the indicated mature B cell subsets (gated on B-2 cells; $CD19^{+}CD5^{-}CD138^{-}CD93^{-}$) in the spleen of the indicated genotypes. **c**, Determination of the *Ikzf1* deletion frequency in T1, T2 and mature ($CD93^{-}$)




Europe PMC Funders Author Manuscripts

B cells of the indicated genotypes by intracellular Ikaros staining and flow cytometry. **d**, Immunohistological analysis of spleen sections from 6-week-old MD4 BCR-tg *Ikzf1* $^{B+}$ and MD4 BCR-tg *Ikzf1* $^{B-}$ mice. The sections were stained with anti-IgD (blue), anti-IgM (green) and anti-CD169/MOMA-1 (red) antibodies. A single B cell follicle is shown with its T cell (T), FO B cell (FO) and MZ B cell (MZ) zones. **e**, Flow cytometric analysis of surface IgD and IgM levels on FO and MZ B cells of the indicated genotypes. T1 B cells (dashed line) of the MD4 BCR-tg *Ikzf1* $^{B+}$ genotype are shown for comparison. Data in **b,c,e** are representative of data shown in **a**, which were analyzed in 9 independent experiments. The data in **d** are representative of 2 independent experiments. Statistical data **(a)** are shown as mean values with SEM and were analyzed by one-way ANOVA (Tukey): *$P < 0.03$, **$P < 0.002$, ***$P < 0.0002$, ****$P < 0.0001$. See Source Data for exact description of the mouse numbers ($n$) and $P$ values. Each dot corresponds to one mouse.



Europe PMC Funders Author Manuscripts

Europe PMC Funders Author Manuscripts

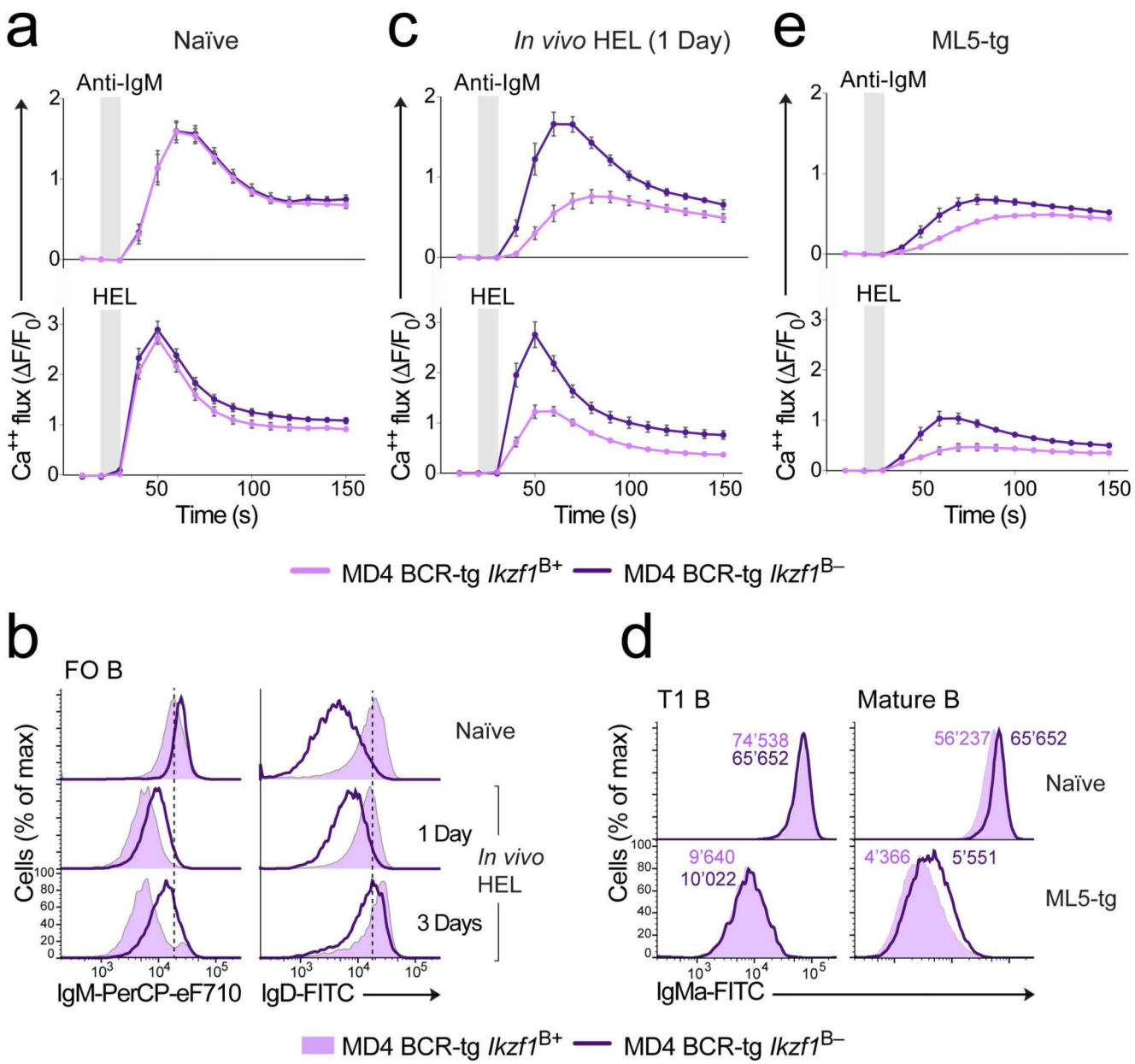


**Fig. 5. Ikaros controls anergy induction and maintenance upon chronic antigen exposure.**

**a**, Calcium mobilization in response to BCR signaling. Intracellular $Ca^{2+}$ fluxes in naïve CD43$^{-}$ FO B cells from lymph nodes of MD4 BCR-tg *Ikzf1* $^{B+}$ (light purple) or MD4 BCR-tg *Ikzf1* $^{B-}$ (dark purple) mice were recorded as an increase of the fluorescent emission of a $Ca^{2+}$ sensor dye after addition (grey shading) of a stimulatory anti-IgM antibody or the cognate antigen HEL. The fluorescence increase is presented as $\Delta F/F_0$ ($F_0$, average fluorescence for 0-20 s before stimulation; $\Delta F$, fluorescence at time 't' - $F_0$). The measurements after anti-IgM or HEL stimulation were averaged over 10 or 12 measurements recorded in 3 or 6 independent experiments, respectively. **b**, Flow cytometric analysis of surface IgD and IgM levels on splenic FO B cells of the indicated genotypes before (naïve) and after injection of the HEL antigen for 1 or 3 days. **c**, Calcium

mobilization in response to anti-IgM or HEL stimulation of $CD43^{-}$ FO B cells from lymph nodes of MD4 BCR-tg *Ikzf1* $^{B+}$(light purple) or MD4 BCR-tg *Ikzf1* $^{B-}$ (dark purple) mice, which were inject one day before with HEL antigen. $Ca^{2+}$ fluxes after IgM or HEL stimulation were measured as in (**a**) and were averaged over 8 or 12 (MD4 BCR-tg *Ikzf1* $^{B+}$) and 4 or 8 (MD4 BCR-tg *Ikzf1* $^{B-}$) measurements recorded in 3 or 4 independent experiments, respectively. **d**, Flow cytometric analysis of surface IgD and IgM levels on naïve splenic T1 B cells and mature B cells ($CD19^{+}CD5^{-}CD138^{-}IgD^{+}CD93^{-}$) of MD4 BCR-tg *Ikzf1* $^{B+}$ or MD4 BCR-tg *Ikzf1* $^{B-}$ mice (top row) as well as on anergic T1 and mature B cells of ML5-tg MD4 BCR-tg *Ikzf1* $^{B+}$ or ML5-tg MD4 BCR-tg *Ikzf1* $^{B-}$ mice (bottom row). Numbers refer to the mean fluorescence intensity measured. Analysis of the intracellular Ikaros levels is shown for T1 and mature B cells of all 4 genotypes in Supplementary Fig. 5c. **e**, Calcium mobilization in response to anti-IgM or HEL stimulation of $CD43^{-}$ FO B cells from lymph nodes of ML5-tg MD4 BCR-tg *Ikzf1* $^{B+}$(light purple) or ML5-tg MD4 BCR-tg *Ikzf1* $^{B-}$ (dark purple) mice, as described in (**a**). The $Ca^{2+}$ measurements after IgM or HEL stimulation were averaged over 5 or 7 measurements, respectively, recorded in 2 independent experiments. Data in **b** and **d** are representative of 5 and 8 independent experiments, respectively. Statistical data **(a,c,e)** are shown as mean values with SEM.

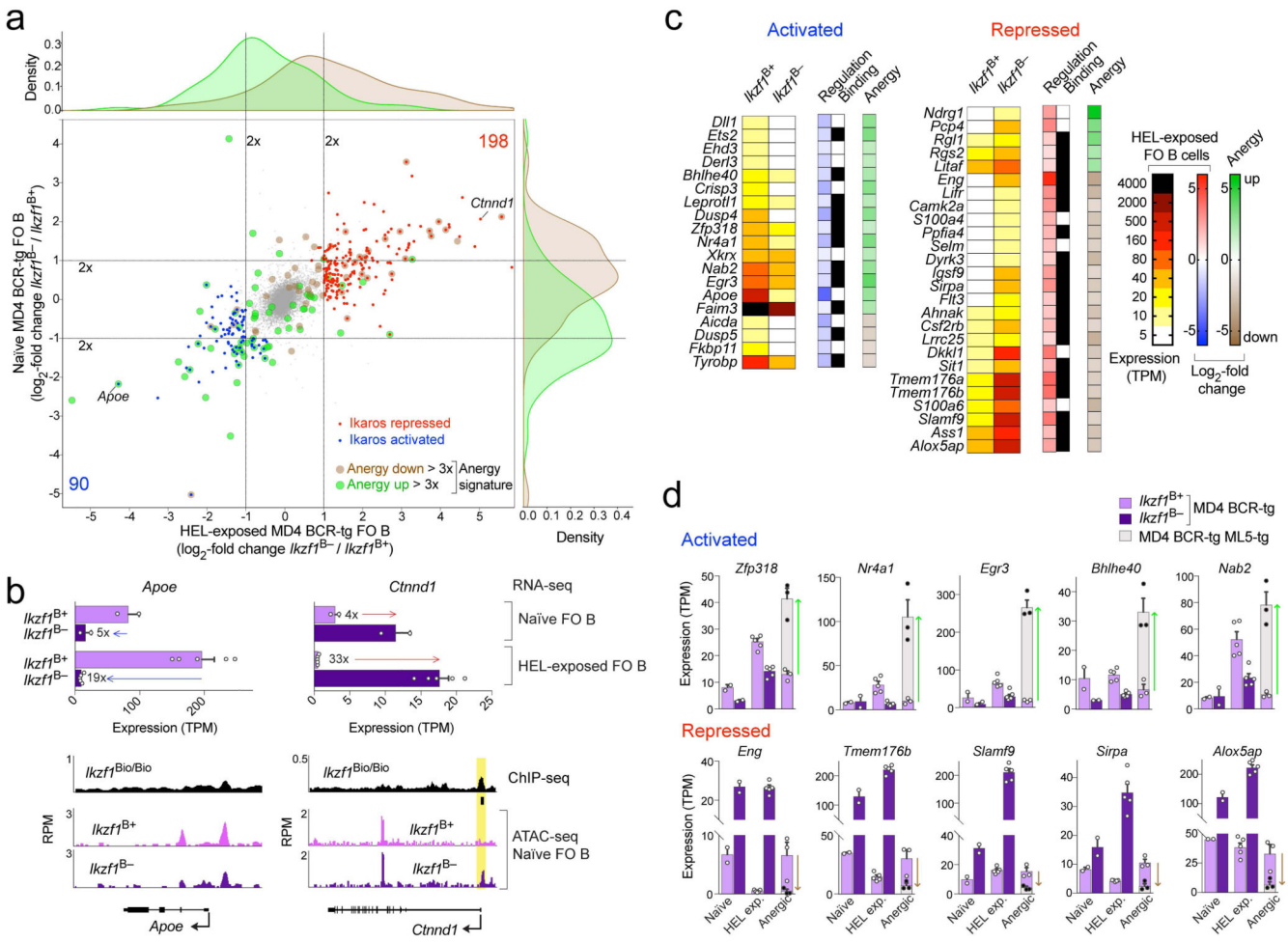


**Fig. 6. Ikaros-dependent gene regulation in anergic B cells.**

**a**, Overlap of the Ikaros-dependent gene expression patterns between naïve and 1-day HEL-exposed FO B cells resulted in a total of 90 Ikaros-activated (blue dots) and 198 Ikaros-repressed (red dots) genes (Table 3). The $\log_2$-fold expression change observed between HEL-exposed Ikaros-deficient (MD4 BCR-tg *Ikzf1* $^{B-}$) and control (MD4 BCR-tg *Ikzf1* $^{B+}$) FO B cells (horizontal axis) as well as between naïve Ikaros-deficient and control FO B cells (vertical axis) is plotted for each gene. Ikaros-regulated genes, which were identified in naïve and HEL-exposed FO B cells (Supplementary Fig. 6c,d), were combined and selected for an adjusted *P* value of < 0.05 in HEL-exposed FO B cells, while genes regulated in opposite directions in naïve and HEL-exposed FO B cells were eliminated (see Online Methods). Genes of the anergy expression signature, which were defined by an expression difference of > 3-fold between fully anergic MD4 BCR-tg ML5-tg FO B cells and naïve MD4 BCR-tg FO B cells (Table 4), are additionally indicated by green dots (upregulated in anergic B cells) and brown dots (downregulated in anergic B cells). Density profiles indicate the Ikaros dependency of the anergy signature genes in HEL-exposed FO B cells (top) or naïve FO B cells (right). **b**, Expression of the Ikaros-activated *Apoe* gene and Ikaros-repressed *Ctnnd1* gene in control (MD4 BCR-tg *Ikzf1* $^{B+}$, light purple) and Ikaros-deficient (MD4 BCR-tg *Ikzf1* $^{B-}$, dark purple) naïve and HEL-exposed FO B cells, as measured by




Europe PMC Funders Author Manuscripts

RNA-seq (upper part). Ikaros binding (black) was determined by Bio-ChIP-seq analysis of naïve *Ikzf1* $^{ihCd2/ihCd2}$ *Rosa26* $^{BirA/BirA}$ FO B cells (black), and open chromatin regions were mapped by ATAC-seq of control (MD4 BCR-tg *Ikzf1* $^{B+}$, light purple) and Ikaros-deficient (MD4 BCR-tg *Ikzf1* $^{B-}$, dark purple) naïve FO B cells (lower part). The Ikaros peak (horizontal bar, yellow shading) at the *Ctnnd1* promoter was defined by 'peak calling'. RPM, reads per million mapped sequence reads. **c**, Heat map displaying the expression of genes that are regulated by Ikaros in HEL-exposed FO B cells and are part of the anergy expression signature. The expression values (TPM) of these regulated genes in Ikaros-deficient and control HEL-exposed FO B cells, their $\log_2$-fold changes in these two cell types (regulation) as well as the $\log_2$-fold changes determined in fully anergic versus naïve FO B cells (anergy) are displayed according to the indicated color keys (right). Black squares denote Ikaros binding at the specified genes in naïve FO B cells. **d**, Expression of the indicated genes in naïve or HEL-exposed Ikaros-deficient FO B cells (dark purple) and in naïve or HEL-exposed control FO B cells (light purple). Gray bars display expression in fully anergic MD4 BCR-tg ML5-tg FO B cells, while the light purple bar overlaid on the gray bar indicates the corresponding expression in naïve MD4 BCR-tg FO B cells. The RNA-seq data shown in **a-d** were obtained from 2 (naïve FO B cells), 5 (HEL-exposed FO B cells) and 3 (anergic FO B cells) independent experiments. The ChIP-seq data in **b** represent the average values of 4 independent experiments. Statistical data (**b,d**) are shown as mean values with SEM.

Europe PMC Funders Author Manuscripts

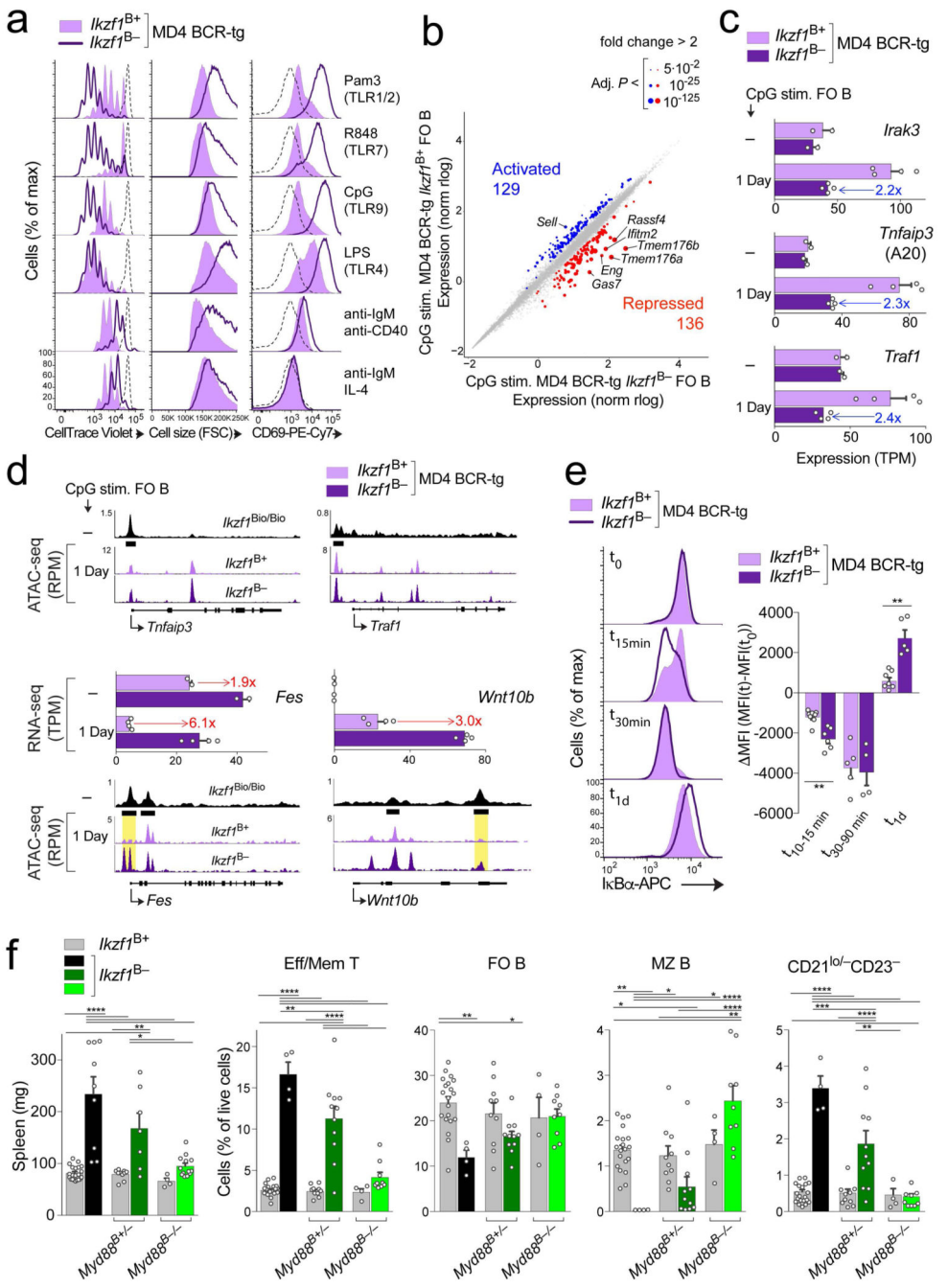


**Fig. 7. Ikaros restrains TLR signaling in B cells.**

**a**, Hyperactivation of TLR signaling in Ikaros-deficient FO B cells. CD43⁻ FO B cells from lymph nodes of *Ikaros* mutant (MD4 BCR-tg *Ikzf1* $^{B-}$; dark purple line) and control (MD4 BCR-tg *Ikzf1* $^{B+}$; light purple) mice were stained with the CellTrace Violet reagent before stimulation with Pam3, R848, CpG, LPS, anti-IgM plus anti-CD40 or anti-IgM plus IL-4 for 4 days followed by flow cytometric analysis of the CellTrace Violet staining pattern, the cell size and CD69 expression. Dashed lines refer to unstimulated *ex vivo* FO B cells of MD4 BCR-tg *Ikzf1* $^{B+}$ mice. **b**, Scatterplot of gene expression difference between Ikaros-deficient

(MD4 BCR-tg *Ikzf1* $^{B-}$) and control (MD4 BCR-tg *Ikzf1* $^{B+}$) FO B cells that were stimulated with CpG for 1 day. Ikaros-activated genes (blue dots) and Ikaros-repressed genes (red dots) were defined by an expression difference of > 2-fold, an adjusted *P* value of < 0.05 and a TPM value of > 5 in Ikaros-deficient or control B cells, respectively (Table 5). **c**, Expression of the activated Ikaros target genes *Irak3, Tnfaip3* and *Traf1* in control (light purple) and Ikaros-deficient (dark purple) FO B cells before (naïve) and after 1 day of CpG stimulation, as measured by RNA-seq analysis. **d**, Ikaros binding and open chromatin regions at activated (*Tnfaip3* and *Traf1*) and repressed (*Fes* and *Wnt10a*) Ikaros target genes, as determined by Bio-ChIP-seq of naïve FO B cells (black) and ATAC-seq of control (MD4 BCR-tg *Ikzf1* $^{B+}$, light purple) and Ikaros-deficient (MD4 BCR-tg *Ikzf1* $^{B-}$, dark purple) FO B cells after 1 day of CpG stimulation. The expression of *Fes* and *Wnt10b* before (naïve) and after 1 day of CpG stimulation is additionally shown, as described in **c**. Yellow shading indicates Ikaros-binding regions, where open chromatin is only induced upon loss of Ikaros. **e**, Altered oscillation of NF-κB activity upon TLR9 stimulation in Ikaros-deficient FO B cells, as shown by IκBα degradation. The amount of IκBα protein was determined by intracellular flow staining of Ikaros-deficient (dark purple, $n = 6$) and control (light purple, $n = 8$) FO B cells before ($t_0$) and after 15 min, 30 min or 1 day of CpG stimulation (left). The flow cytometric data were quantified (right) by displaying the difference in median fluorescence intensity (MFI(t) – MFI($t_0$)) at the indicated time points for CpG-stimulated FO B cells analyzed from multiple mice (indicated by dots). **f**, Determination of the spleen weight and relative abundance of the indicated splenic T and B cell types in control *Ikzf1* $^{B+}$ mice (gray, without or with *Myd88* $^{B+/-}$ or *Myd88* $^{B-/-}$, $n = 4$-21), *Ikzf1* $^{B-}$ mice (black, $n = 4$-9), *Myd88* $^{B+/-}$ *Ikzf1* $^{B-}$ mice (*Cd23*-Cre *Myd88* $^{+/fl}$ *Ikzf1* $^{fl/fl}$, dark green, $n = 7$-11) and *Myd88* $^{B-/-}$ *Ikzf1* $^{B-}$ mice (*Cd23*-Cre *Myd88* $^{fl/fl}$ *Ikzf1* $^{fl/fl}$; light green, $n = 9$-13) at the age of 5-10 weeks. Data in **a** are representative of 4 (Pam3, R848), 6 (CpG), 7 (LPS) and 3 (anti-IgM plus anti-CD40 and anti-IgM plus IL-4) independent experiments. The RNA-seq data shown in **b-d** were obtained from 2 (naïve FO B cells) and 4 (CpG-stimulated FO B cells) independent experiments. The ChIP-seq data in **d** represent the average values of 4 independent experiments. Data in **e** and **f** are based on 5 and 7 independent experiments, respectively. The statistical data **(c-f)** are shown as mean values with SEM and were analyzed by multiple *t*-tests (unpaired, two-tailed, Holm-Sidac; **e**) or by one-way ANOVA (Tukey; **f**): * $P < 0.03$, ** $P < 0.002$, *** $P < 0.0002$, **** $P < 0.0001$. See Source Data for exact description of the mouse numbers (*n*) and *P* values. Each dot (**c-f**) corresponds to one mouse.




Europe PMC Funders Author Manuscripts